Lithos 334–335 (2019) 231–244

Contents lists available at ScienceDirect

Lithos

journal homepage: www.elsevier.com/locate/lithos

Mineralogical and geochemical constraints on the origin and evolution of albitites from Dmytrivka at the Oktiabrski complex, Southeast Ukraine

Magdalena Dumańska-Słowik [a,*], Tomasz Powolny [a], Magdalena Sikorska-Jaworowska [b], Wiesław Heflik [a], Vyacheslav Morgun [c], Ban To Xuan [d]

[a] Faculty of Geology, Geophysics and Environmental Protection, AGH University of Science and Technology, 30 Mickiewicz avenue, 30-059 Krakow, Poland
[b] Polish Geological Institute - National Research Institute, 4 Rakowiecka street, 00-975 Warsaw, Poland
[c] M.P. Semenenko Institute of Geochemistry, Mineralogy and Ore Formation, National Academy of Science of Ukraine, 34 Acad. Palladina avenue, 03680 Kiev, Ukraine
[d] Faculty of Geosciences and Geoengineering, Hanoi University of Mining and Geology, 18 Pho Vien street, Bac Tu Liem district, Hanoi, Viet Nam

ARTICLE INFO

Article history:
Received 11 February 2019
Accepted 20 March 2019
Available online 23 March 2019

Keywords:
Albitite fenitization
Metasomatism
Zircon glomerocrysts
Tetrad effect

ABSTRACT

Albitites from Dmytrivka quarry form veins like bodies within fenitized alkali granites of the Oktiabrski complex. They are mainly composed of albite, and subordinately K-feldspar, zircon, aegirine, astrophyllite, pyrochlore and ilmenite. Albitites are characterized by high alkalies ($Na_2O + K_2O$) content coupled with low MgO, CaO, and SiO_2 concentrations relative to host alkali granites. They show inversion of REE patterns (negative slopes for LREE and positive slopes for HREE), enrichment in HFSE (i.e. Zr, Nb, Ta), and strong Eu anomalies. The existence of rare composite of M-type and W-type REE tetrad effect in albitites indicates their complex genesis, i.e. formation during the coexistence of the melt with aqueous phase, later being superimposed by further alterations with hydrothermal solutions. The magmatic origin of albitites (evolved from highly differentiated A-type magma and emplaced at shallow depths) is documented by the presence of flow and snowball textures, zircon-aegirine glomerocrysts, no traces of replacement interfaces and reaction zones between K-feldspar and albite as well as no smooth, gradual changes in bulk-rock compositions between alkali granite, fenite vs albitite. On the contrary, the strong influence of pervasive, post-magmatic high-temperature (381–392 °C evidenced by CM geothermometer), and highly-oxidizing alkaline-bearing metasomatizing fluids on albitites is revealed by the occurrence of polygonal textures of albite laths, red CL luminescence of feldspars typical of fenitized rocks as well as crystallization of astrophyllite at the expense of arfvedsonite. Additionally, the presence of fluid-mineral interactions is evidenced by the development of secondary porosity and patchy zoning within zircon crystals coupled with the presence of blue (Dy^{3+}-Tb^{3+}-activated) and yellow (SiO_4-Tb^{3+}-activated) domains within them. All these textural, mineralogical and geochemical features observed in albitites from Dmytrivka suggest complex, magmatic-hydrothermal nature of the rocks.

1. Introduction

Albitites (also called albitic or albite rocks) represent very uncommon and enigmatic rocks of a quite simple mineralogical composition dominated by albite (70–80% vol%) accompanied by subordinate amounts of quartz, K-feldspar, mica, apatite, zircon, and titanite (e.g. Castorina et al., 2006; Mohammad et al., 2007). They are found in several geological settings such as magmatic, hydrothermal units or in association with metamorphic rocks - i.e. amphibolite, granulite, and blueschist facies (e.g. Azer et al., 2010; Engvik et al., 2014; Mohammad et al., 2007; Pin et al., 2006).

The largest albitite occurrences in Europe are located at Otana-Sarule-Orani-Oniferi area in Central Sardinia, Italy (Castorina et al., 2006; Palomba, 2001). These outcrops cover an area of 90 km^2, where the albitites form lenses or vein-shaped bodies along fractures of Variscan granodiorites (Castorina et al., 2006; Palomba, 2001). In south Norway albitites are reported from the Sveconorwegian Bamble Sector composed of medium- and high-grade metamorphic rocks (Engvik et al., 2014). Dikes of pegmatitic albitite intruding serpentinized lherzolite at Urdach and Espechere from the western Pyrenees, France were reported by Pin et al. (2006). In Ukraine albitites host rich uranium

* Corresponding author.
E-mail address: dumanska@agh.edu.pl (M. Dumańska-Słowik).

https://doi.org/10.1016/j.lithos.2019.03.024
0024-4937/

mineralization and occur as zoned metasomatic bodies within gneisses, migmatites and granites of the Ingul Paleoproterozoic terrain in the Ukrainian shield (Shumlyanskyy et al., 2015). Kryvdik (2017) reported the occurrences of apofenitic albitites in the Azov Sea area (Chernigivka carbonatite complex, the fenites of Dmytrivka village, Tunikova valley), and the western part of the Ukrainian shield (Proskurivska complex of alkaline rocks, Beryozovaya Gat's fenites) and in the Middle Dnieper region (Mala Tersa alkaline rocks).

Overall, the exact origin of albitites is still the matter of debate in the world literature of petrology. They could be formed as a result of: (1) metasomatism of granitic rocks by hydrothermal fluids (Cathelineau, 1988, 2) direct precipitation from solution (Johnson and Harlow, 1999), and/or (3) crystallization from sodium enriched magma (Schwartz, 1992). Igneous albitite has been reported very rarely (e.g. Pin et al., 2006), whereas albitites of hydrothermal-metasomatic origin occur much more frequently (e.g. Engvik et al., 2014). However, the recognition of the origin of these rocks is frequently a challenging task, as it requires the application of many advanced analytical techniques combined with careful field observations. Albitites from Dmytrivka form vein-like bodies within pyroxene fenites and granitic rocks. They occur near granitoids, pyroxenites, and mariupolites (albite-aegirine nepheline syenite) belonging to the Oktiabrski alkaline complex (SE Ukraine). In this contribution we present a detailed characteristics of albitites from the Dmytrivka quarry based on combined conventional optical microscopy, cathodoluminescence, and scanning electron microscopy (SEM-EDS) supported by Raman microspectroscopy and bulk-rock analyses. Our research provides insights into the origin of these rocks and focuses on fluid-mineral interaction during their evolution. We also discuss a petrogenetic relationships between albitites and alkali granite-fenite association from the Oktiabrski complex to trace and pinpoint the various stages of metasomatic alterations.

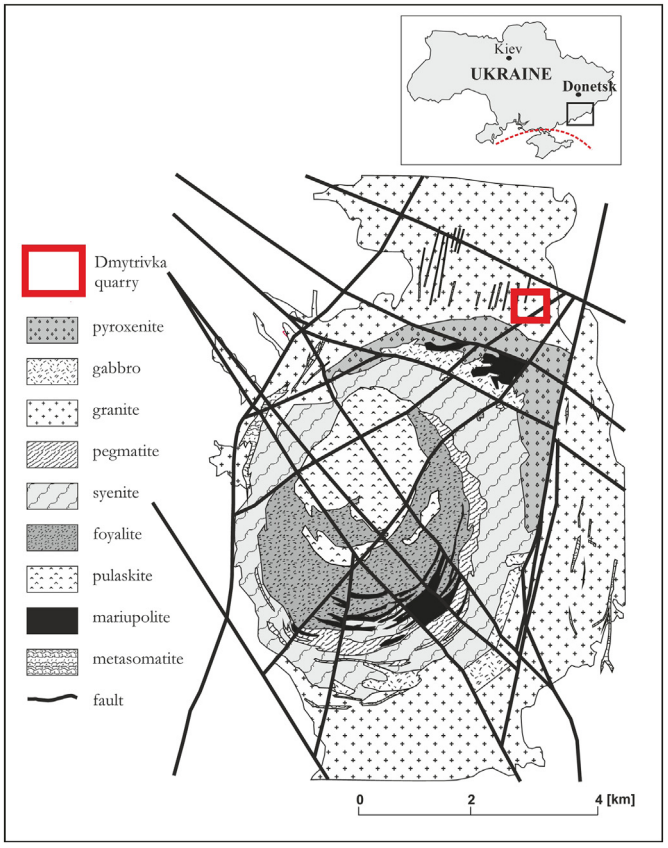

Fig. 1. Simplified geological map of the Oktiabrski alkaline ring complex with the locality of Dmytrivka quarry.
Modified after Dumańska-Słowik et al. (2011).

2. Geology settings

The Oktiabrski alkaline complex (Priazov block of the Ukrainian Shield), which is a part of a unique province of alkaline magmatism of Proterozoic age ca. 1.8 Ga (U-Pb zircon method; Volkova, 2000, 2001; Ponomarenko et al., 2013) is situated approximately 3 km south of Volnovakha and 50 km south-east of Donetsk (south-eastern Ukraine). It was formed at the platform stage of the Ukrainian Shield development and is associated with a system of deep faults (Sviridov, 1973). Now it is situated at the border line between the Volodarsk and the Oktiabrski deep faults. Such localization resulted in formation of block-style structure of the complex (Volkova, 2001).

It is oval-shaped with an N-S elongation and covers the area of 34 km^2. It has a somewhat irregular concentric structure: in the centre there are *pulaskites,* i.e., nepheline-bearing alkali feldspar syenites with variable proportions of dark minerals such as Na-bearing pyroxenes and amphiboles, fayalite and biotite, which are surrounded by foyaites. The latter are in turn enclosed by syenites. *Mariupolites*, the nepheline albite-aegirine syenites, forming veins of various thickness from a few centimetres to meters (Yanchenko et al., 2010), occur in the periphery of this alkaline complex. They occur in the vicinity of peridotites, pyroxenites and gabbros, which are the oldest rocks in the complex (Volkova, 2001), or foyaites and pegmatites. Granitoid rocks are found only in the peripheral parts of the alkaline complex (Fig. 1).

The genesis of this alkaline complex has been debated for a long time. Tichonienkova et al. (1967) suggested that the rocks of the Oktiabrski complex were formed as a result of post-magmatic and metasomatic alteration processes. The presence of fenites in the vicinity of the complex (Khlibodarivka, Dmytrivka, Petrovo-Hnutovo) supports this theory. Donskoy (1982) and Solodov (1985) suggested that a majority of the rocks crystallized due to differentiation of magma with the composition of nepheline syenite. However, they also agreed that metasomatic activity that affected the rocks of this complex was responsible for significant concentration of rare metals such as Nb, Zr and REEs (Volkova, 2001).

Dmytrivka quarry is located at north-eastern periphery of the Oktiabrski complex. Albitites form vein-like bodies within fenitized granitoides in the close neighbourhood with pyroxenites and mariupolites (Fig. 1). These bodies are marked by sharp contacts with adjacent rocks and reach up to a few meters in thickness.

3. Analytical methods

Polished thin sections of albitites, fenites and granites were investigated using Olympus BX51 polarizing microscope with a magnification range from 40 to 400 times. The photomicrographs were taken using Olympus DP12 digital camera linked to Analysis software.

The cathodoluminescence analyses of albitites were conducted at the Polish Geological Institute - National Research Institute in Warsaw. The CL observations were performed on polished thin sections using a Cambridge Image Technology CCL 8200 MK3 device (cold cathode), coupled with Nikon Optiphot 2 polarizing microscope, and equipped with digital Canon EOS 600D camera. The scanning electron microscopy with cathodoluminescence (SEM-CL) analyses utilised a LEO 1430 scanning electron microscope coupled with CL-image system (ASK-CL VIS Viev) and CL spectrometer (ASK SEM-CL). The system operated in a high-vacuum mode, at 20 kV accelerating voltage, and 50 μA current. The intensity of CL spectra were normalized to 100% in terms of the intensity units.

Back-scattered electron (BSE) observations of albitites were conducted at Faculty of Geology, Geophysics and Environmental Protection, AGH, on polished thin sections using a FEI Quanta 200 FEG scanning electron microscope equipped with EDAX energy dispersive spectrometer (EDS). The system operated at 25 kV accelerating voltage, 50 μA

current, in a high-vacuum mode, i.e. 6×10^{-5}-7×10^{-6}Torr. The quantitative analysis of target elements, based on relative peak intensity calculated from EDS spectrum, were supported by ZAF correction.

Raman spectra of selected mineral components of albitites, as well as solid and fluid inclusions in albite crystals were recorded on clean cleavage surfaces of the rocks and double polished wafers, respectively using a Thermo Scientific DXR Raman microscope featuring 10×, 50× and 100× magnification objectives. The samples were excited with a 532-nm laser with power from 10 to 20 mW; exposure time was 3 s, the number of exposures was 10, and the laser focus diameter was approximately 2–1 μm. The spectra were corrected for background by the sextic polynomial method using Omnic software. The Raman spectra of carbonaceous material found as inclusions within albite were reordered using low laser power (1–2 mW) in order to avoid heating effects. Regarding the fact the polishing procedure may change the shape of Raman spectra (e.g. Beyssac et al., 2003), the microscope was not focused on sample surface and the signal was acquired using in-depth analysis (confocal mode). The acquisition time was 30 s. The deconvolution was performed by Thermo Scientific *OMNIC* Spectra Software following the procedure proposed by Kouketsu et al. (2014), whose worked out the CM geothermometer applicable to temperatures in the range of 150–400 °C. All obtained spectra were corrected for fluorescence by subtracting a linear baseline in the range of 1000–1750 cm^{-1}. The spectra were decomposed into 3 bands (G, D1, and D2) using pseudo-Voigt (Gaussian-Lorentzian sum) function. The metamorphic temperatures were estimated using the full-width half measured of D1 band on the basis of the equation: $T(°C) = -2.15 \cdot FWHM\text{-}D1 + 478$.

The whole-rock analyses were carried out at Bureau Veritas Minerals Laboratories Ltd. in Vancouver Canada, using LF200 package. The material of 5 g per each sample was crushed in an agate mortar and sieved before analysis. Samples were then mixed with LiBO2/Li2B4O7 flux. Crucibles were fused in a furnace. The cooled bead was dissolved in ACS grade nitric acid and analysed by combined ICP-OES (Inductively Coupled Plasma - Optical Emission Spectrometry) and ICP-MS (Inductively Coupled Plasma - Mass Spectrometry). Major and trace element compositions were acquired using Spectro Ciros Vision and ELAN 9000 devices, respectively. Loss on ignition (LOI) was measured by igniting a sample split and measuring the weight loss.

4. Results

4.1. Optical microscopy observations and petrography

4.1.1. Granite

The rock is characterized by non-foliated, medium-grained, and inequigranular textures. It is predominately composed of alkali-feldspar, plagioclases, and quartz, but also contains subordinate amounts of mafic minerals (biotite and alkali-amphiboles). Plagioclases form hypidiomorphic laths up to ca. 1.5 mm long that frequently exhibit polysynthetic twinning lamellae. Some of the crystals are locally covered by aggregates of white mica (sericite). Microcline occurs as large (up to 3 mm size) and well-preserved crystals with blocky habit that commonly reveal the presence of cross-hatched pattern, as well as irregular perthitic intergrowths (Fig. 2A). Some of the microclines were converted into co-oriented chessboard albite, which is relatively fresh as compared with plagioclases (Fig. 2B–C). Quartz appears as xenomorphic crystals with undulose extinction that fill the interstitial spaces between alkali-feldspars and plagioclases. Mafic minerals of granite are mainly represented by biotite forming flakes up to ca. 1 mm long. Biotite is partially altered into bluish to greenish alkali-amphiboles (arfvedsonite and/or riebeckite) (Fig. 2D). Small zircon, apatite crystals and opaque minerals were recognized as major accessory phases within rock matrix.

4.1.2. Fenite

The texture of this rock is non-foliated, fine-grained to medium grained, and inequigranular. The rock matrix is dominated by an albite-aegirine assemblage, with lesser amounts of alkali-amphiboles, quartz, and microcline. Albite forms xenomorphic laths of variable size (up to 0.3 mm long). These crystals often display embayed contacts referred as triple-point junctions. Numerous alkali-amphiboles (arfvedsonite/riebeckite) are found within rock matrix where they occupy interstitial space between feldspars. Some of them seem to be

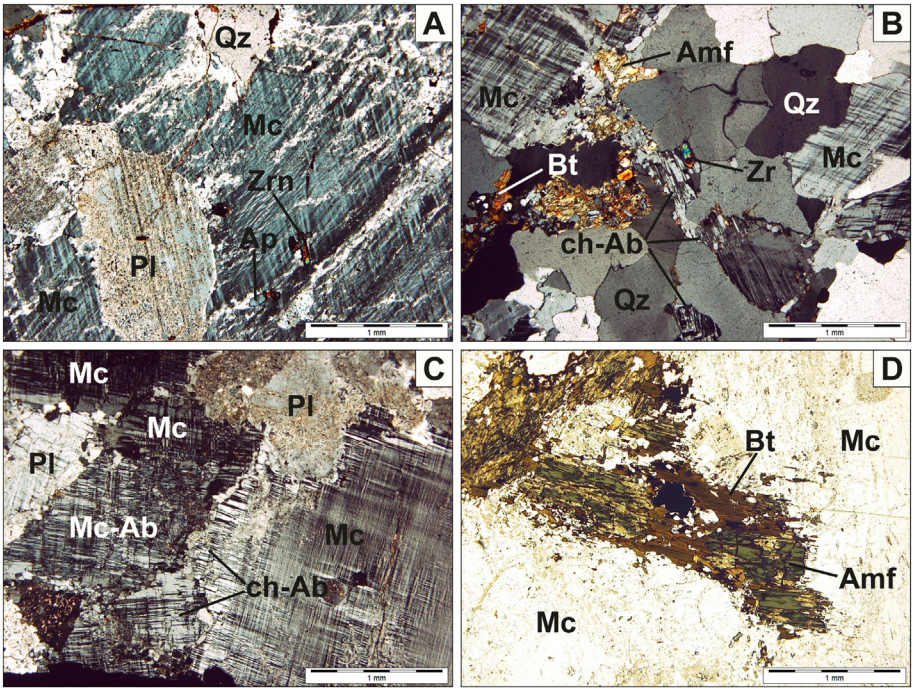

Fig. 2. Photomicrographs of granite samples. (A) Cross-hatched microcline (Mc) with perthitic intergrowths accompanied by weathered plagioclase laths (Pl) and quartz (Qz). Note the presence of inclusions made of apatite (Ap) and zircon (Zr) within microcline - PX; (B-C) Cross-hatched microcline partially altered to albite exhibiting chessboard twinning pattern (ch-Ab) -PX; (D) Progressive replacement of biotite (Bt) by alkali-amphiboles (Amf) - 1 N.

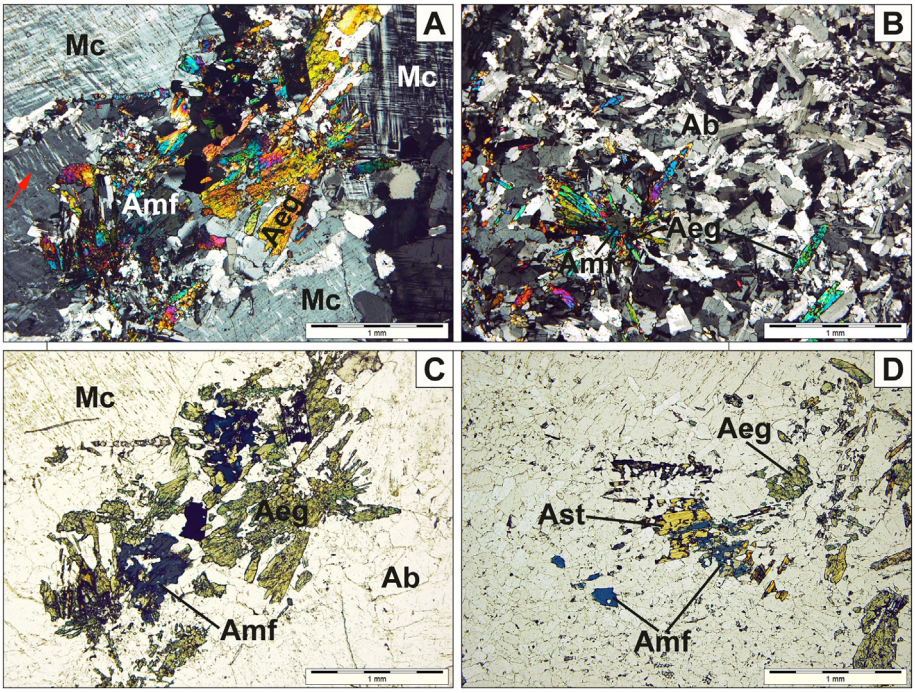

Fig. 3. Photomicrographs of fenite samples. (A) Aegirine and alkali-amphiboles accompanied by microcline. Note the presence of flame perthite within microcline (red arrow) -PX; (B) Aegirine grouped in radial concretions surrounded by numerous albite plates -PX; (C) The replacement of alkali-amphiboles by aegirine - 1 N; (D) The replacement of alkali-amphiboles by astrophyllite - 1 N. (For interpretation of the references to colour in this figure legend, the reader is referred to the web version of this article.)

partially transformed into aegirine, which occurs as either elongated prisms up to 0.5 mm long or radial concretions (Fig. 3A–C). Moreover, subordinate astrophyllite with distinctive bronze-yellow to golden-yellow pleochroism appears as the product of alteration of alkali-amphiboles (Fig. 3D). Microcline occurs in the same form as in the granite samples. Nevertheless, some of the crystals contain flame perthites (absent in granite samples). Zircon represents a major accessory phase of the rock. Minor secondary chlorites and Fe-O oxides form veins that cut across the rock matrix.

4.1.3. Albitite

The texture of the rock could be described as equigranular (medium- to fine-grained), granoblastic, and glomeroblastic. As the name implies, albitite is mostly composed of Na plagioclase (albite)

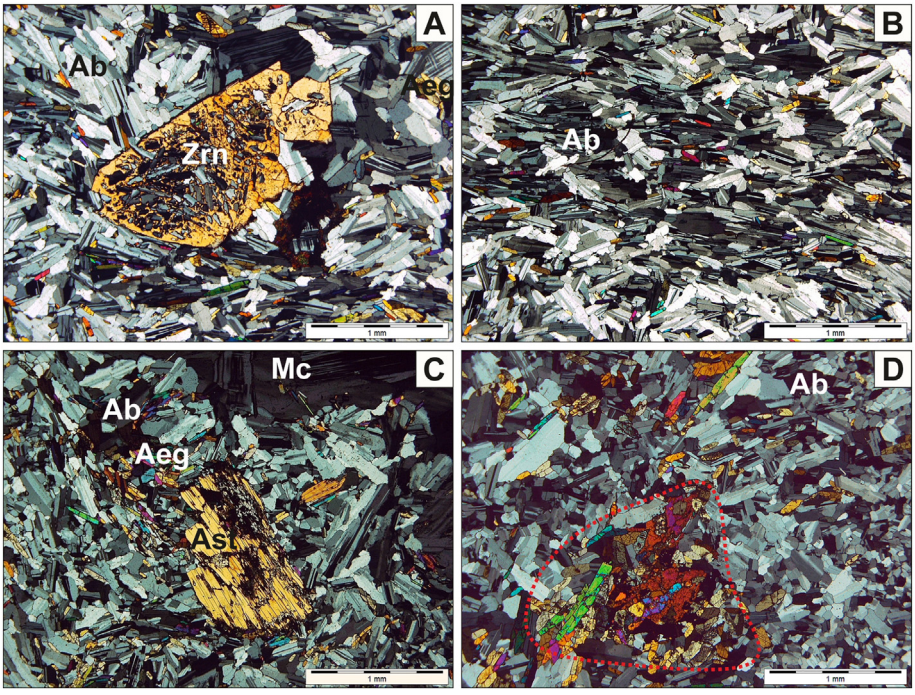

Fig. 4. Photomicrographs of albitite samples. (A) Zircon (Zr) containing numerous inclusions of albitite (Ab) forming so-called snowball texture - PX; (B) Linear arrangement of albitite laths (Ab) accompanied by aegirine (Aeg) - PX; (C) Astrophyllite (As) accompanied by albite, aegirine, and microcline (Mc) - PX; (D) Zircon-aegirine glomerocryst (marked by red dotted line) surrounded by xenomorphic albitic laths sharing triple junctions of ca. 120°- PX. (For interpretation of the references to colour in this figure legend, the reader is referred to the web version of this article.)

forming either non-turbid euhedral plates up to 0.4 mm long or fine-grained aggregates with anhedral shape. Albite laths, which are commonly embedded within microcline and zircon, slightly resemble so-called snowball texture (Fig. 4A). Some of the crystals locally reveal a subparallel arrangement within rock matrix (Fig. 4B). Albites frequently exhibit straight grain boundaries with interfacial angles of ca. 120° (triple-point junctions) (Fig. 4C–D). They are also accompanied by relatively large (up to 1.0 mm) cross-hatched microcline, as well as numerous acicular pyroxenes (aegirine) and subordinate astrophyllite (Fig. 4C). The latter occurs as flattened prismatic crystals or small shreds irregularly scattered within rock matrix. Zircon forms a relatively large (up to ca. 0.2 mm) crystals with anhedral and rounded shape. However, the vast majority of zircons occur as clusters of numerous grains, which could be described as glomerocrysts (Fig. 4D). These glomerocrysts amount ca. 1.0 mm in diameter. Not only are they composed of single zircon grains, but comprise opaque minerals and aegirine.

SEM-BSE images revealed that albite crystals appear fairly homogenous and exhibit lack of any secondary porosity (Fig. 5A). They are also characterized by chemical purity reflected by extremely low K and Ca content. Zircon glomerocrysts display mosaic micro-texture (patchy zoning) as well as high micro-porosity and fracturing (Fig. 5B–D). They are locally associated with ilmenite-pyrophanite and frequently contain small (up to 0.1 mm size) inclusions comprising Nb-rich phases recognized as pyrochlore. Additionally, some of the zircons seem to exhibit poorly-developed oscillatory zonation as presented in the Fig. 5D.

4.2. Cathodoluminescence microscopy and spectroscopy (OM-CL) of albites

Cathodoluminescence observations indicated that plagioclases and alkali feldspars exhibit various CL colours. Both generations of albite (larger and smaller crystals) luminescence in red colours (Fig. 6A–B), characterized by intensive emission line at 721–725 nm activated by Fe^{3+} (Götze, 2000; White et al., 1986). The weak line at 455 nm is due to Al-O^{-}-Al centre (Fig. 6C).

K-feldspars, with relatively homogenous composition, occurring in albitites exhibit various CL colours: grey-blue, blue, brown, pink and brown-red. Their CL spectra are characterized by emission lines found in blue region at 400–466 nm and the red range of 659–692 nm (Fig. 6D). The CL emission bands found in blue region are caused by Ti^{4+} activator forming Al-O^{-}Ti emission centre (ca. 430 nm vide Kayama et al., 2010) and paramagnetic defect caused by substitution of Al^{3+} for Si^{4+} in feldspar structure and formation of Al-O^{-}-Al centre (ca. 450–470 nm vide Götze, 2000). The red emission bands are attributed to Fe^{3+} occupying Al^{3+} tetrahedral sites in feldspar structure (Götze, 2000; White et al., 1986). The relative intensities of the bands found in blue and red region differ between K-feldspar showing various CL colours (Fig. 6D). The most intensive line due to Al-O^{-}-Al was recorded for blue and grey-blue luminescent K-feldspars, whereas distinct peak attributed to Fe^{3+} was noted for nearly all CL luminescent alkali feldspars. The less intensive emission lines in red region was recorded for K-feldspar with dark brown CL.

Zircon crystals are strongly fractured and show irregular domains with yellow cathodoluminescence colours. Among these regions,

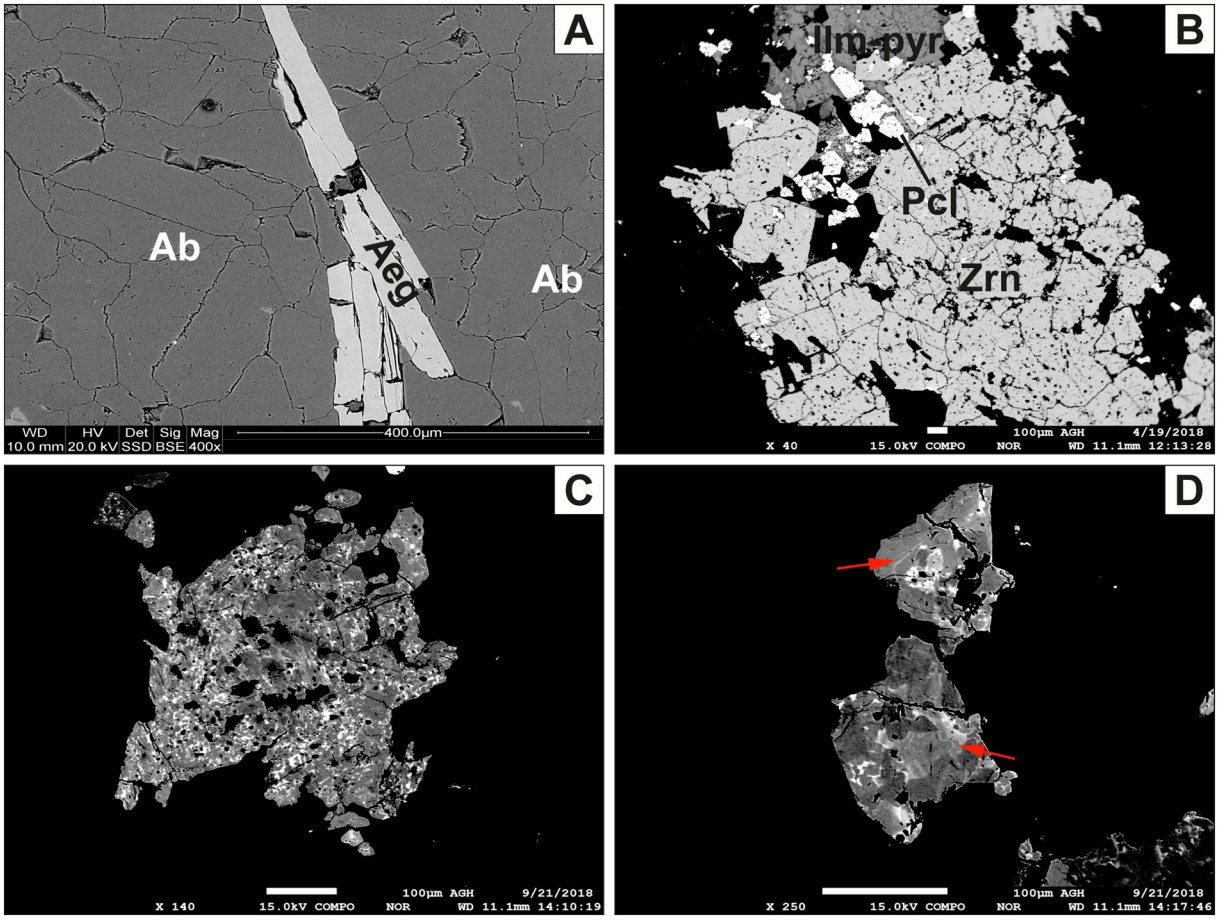

Fig. 5. SEM-BSE images of albitie samples. (A) aegirine (Aeg) surrounded by unzoned and chemically pure albite crystals; (B-D) Glomerocrysts made of zircon accompanied by ilmenite-pyrophanite (Ilm-Pyr) and pyrochlore (Pcl); Note the presence of microporosity and patchy zoning within zircon crystals (D-E), as well as traces of oscillatory zonation (F, indicated by red arrow). (For interpretation of the references to colour in this figure legend, the reader is referred to the web version of this article.)

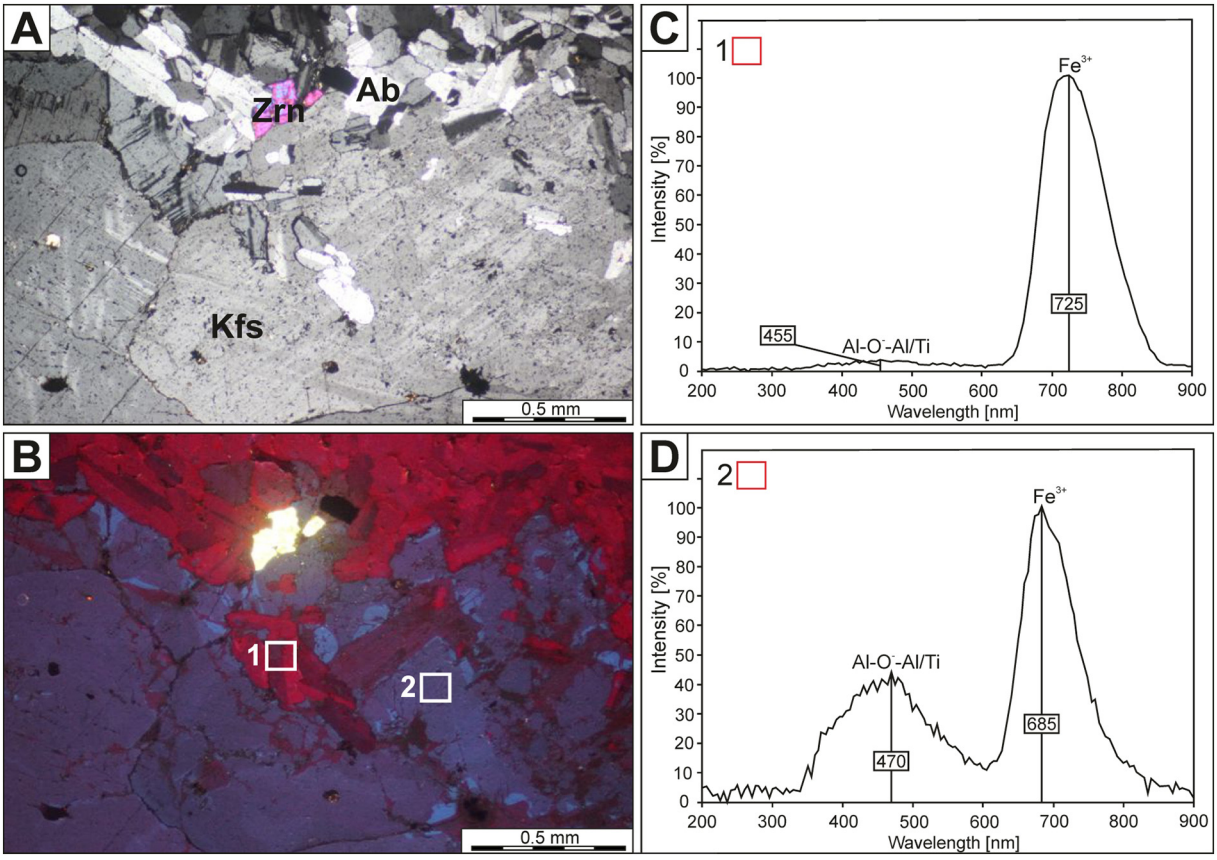

Fig. 6. Photomicrograph (A) and corresponding CL image (B) of albitite sample revealing the presence of red-luminescent albite (Ab) and blue-luminescent microcline (Kfs); Note the presence of yellowish zircon (Zr); (C, D) CL spectra in the range of 200–900 nm taken from of red-luminescent albite (C) and blue-luminescent K-feldspar (D). (For interpretation of the references to colour in this figure legend, the reader is referred to the web version of this article.)

dark navy-blue CL coloured regions are observed (Fig. 7A–B). CL emission spectra obtained for the yellow CL domains revealed the presence of intensive lines at 475 and 570 nm (Fig. 7D), both of them activated by Dy^{3+} (Gorobets and Rogojine, 2002; Götze, 2000). The broad emission band at 383 nm and less intensive lines at 534 and 545 nm are the most probable due to Tb^{3+} in zircon structure (Blanc et al., 2000; Gaft et al., 2005). Hence, the yellow CL of zircon seems to be mainly controlled by extrinsic defects such as dysprosium and terbium. The emission spectrum recorded for dark navy-blue CL domains is characterized by two broad bands at 368 and 549 nm (Fig. 7C). The former is attributed to intrinsic defects, whereas the latter is due to Tb^{3+} (Gaft et al., 2005; Gorobets and Rogojine, 2002). The peak at 368 nm is significantly non-symmetrical suggesting this emission line could be also connected with the presence of Tb^{3+} (?). This dull blue luminescence of zircon is mostly activated by lattice defects and Tb^{3+} in zircon structure.

4.3. Raman micro-spectroscopy of albites

The Raman micro-spectroscopy of albitites confirmed the presence of astrophyllite by its strongest marker bands at 918, 715, 654 and 245 cm^{-1} (Fig. 8). The peaks at 918, 715 and also 1030 cm^{-1} could be associated with Si-O stretching vibrations (Agakhanov et al., 2016; Kampf et al., 2010). Other bands at 654, 559, 423, 403, 365, 345 cm^{-1} may be assigned to bending vibrations of silicate groups, and those at 245, 171, 127 cm^{-1} are attributed to lattice vibrations (Agakhanov et al., 2016; Cámara et al., 2017).

The ore minerals found in albite are represented by rutile and hematite. Rutile manifests its presence by diagnostic marker bands at 612, 445 and 142 cm^{-1} attributed to A1g, Eg and B1g, respectively (Fig. 9). The weak and broad band at 244 cm^{-1} is due to second-order scattering feature (Swamy et al., 2006).

The diagnostic Raman bands for hematite are found at 1315, 655, 607, 504, 408, 289, 242, 223 cm^{-1} (Fig. 10). The broad peak located at 1315 cm^{-1} is typical of disordered hematite and should be assigned to a second-order 2LO mode with 2Eu symmetry due to defects in its lattice (Marshall and Marshall, 2013). The other, intensive bands at 607, 408 and 289 cm^{-1} are assigned to Fe-O symmetric bending vibrations (Eg mode), whereas the weaker lines at 504, and 223 cm^{-1} are related to symmetric stretching vibrations of Fe-O (A1g) (Legodi and De Waal, 2006). The occurrence of the bands at 504, 478, 408 and 289 cm^{-1} also proves the presence of albite (McKeown, 2005), which hosts the inclusions of hematite.

The marker bands for zircon occur at 1010, 977, 443, 360, 229, 218 and 206 cm^{-1} (Fig. 11). They are internal modes: 1010 cm^{-1} (B1g, Si-O $\nu 3$ stretching), 977 cm^{-1} (A1g, Si-O $\nu 1$ stretching), and 443 cm^{-1} (A1g, Si-O $\nu 2$ bending) and external modes: 360, 229, 2018 and 206 cm^{-1} (Syme et al., 1977; Yang et al., 2014).

Raman spectra reordered from inclusions hosted by secondary albite revealed the presence of gaseous $^{12}CO_2$, high-grade carbonaceous material (CM), and nitrates (NO_3^-).The Raman spectrum of gaseous $^{12}CO_2$ (Fig. 12) is dominated by 2 prominent bands centred at ca. 1389 cm^{-1} ($2v_2$ mode) and 1284 cm^{-1} (v_1 mode) that represent so-called Fermi doublet (cf. Rosso and Bodnar, 1995). These bands were attributed to the symmetric stretching vibrations of CO_2 molecules and resulted from the resonance effects according to Fermi (1931). Additionally, the small shoulder peak located at ca. 1397 cm^{-1} could be assigned to so-called hot band of $^{12}CO_2$ (see Arakawa et al., 2007).

The Raman spectrum of carbonaceous material is shown on the Fig. 13. It is characterized by the presence of 2 broad bands located at ca. 1352 and 1616 cm^{-1}. The former peak is attributed to disordered

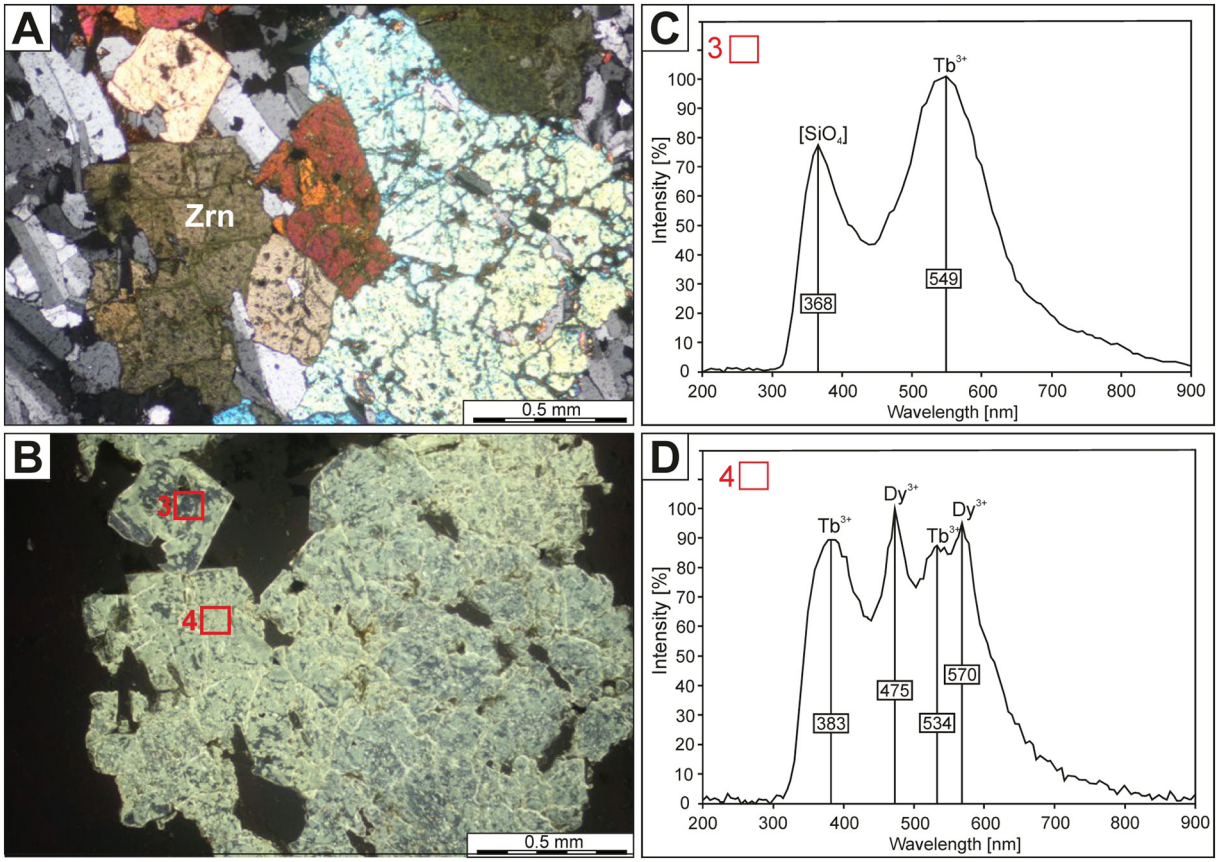

Fig. 7. Photomicrograph (A) and corresponding CL image (B) of albitite sample showing 2 generations of zircons within glomerocrysts: (1) blue-luminescent and (2) yellowish-green-luminescent one; (C, D) CL spectra in the range of 200–900 nm taken from blue-luminescent (C) and yellowish-green-luminescent domains (D) of zircon. (For interpretation of the references to colour in this figure legend, the reader is referred to the web version of this article.)

carbon band (D1) and originates from the presence of defects within the structure of CM (e.g. Wang et al., 1990; Wopenka and Pasteris, 1993; Beyssac et al., 2002; Escribano et al., 2001). On the other hand, the latter peak represents so-called graphitic band (G), which results from in-plane C-C stretching vibrations of well-crystallized carbon (Ferrari and Robertson, 2000; Tuinstra and Koenig, 1970). According to Kouketsu et al. (2014), the relation of intensity between those bands depends on the temperature, at which carbonaceous material has been originally deposited. The predominance of G band over D1 band is typical of the well-crystallized graphite and reflects the presence of a high-grade CM within albitite crystals. The deconvolution of the spectra according to Kouketsu et al. (2014) revealed that FWHM of D1 band falls within the range of 40–45 cm^{-1}, while the corresponding temperature of CM formation could be estimated between 381 and 392 °C, respectively.

Some of the Raman spectra recorded from fluid, liquid inclusions revealed strong band at ca. 1050 cm^{-1} accompanied by weak peak at ca. 690 cm^{-1} indicating the presence of some solutes (Fig. 14). According to Frezzotti et al. (2012), these peaks could be attributed to vibrational bands of nitrates compounds (NO_3^-). Nevertheless, the presence of HSO_4^- also cannot be ruled out since it is characterized by the 1049 cm^{-1} marker band (Burke, 2001).

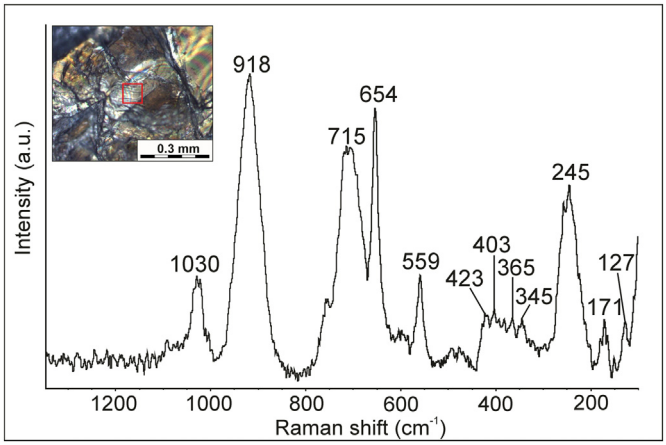

Fig. 8. Raman spectrum of astrophyllite.

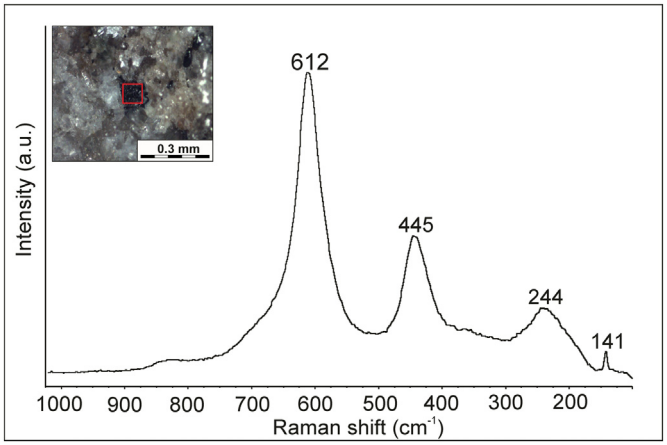

Fig. 9. Raman spectrum of rutile.

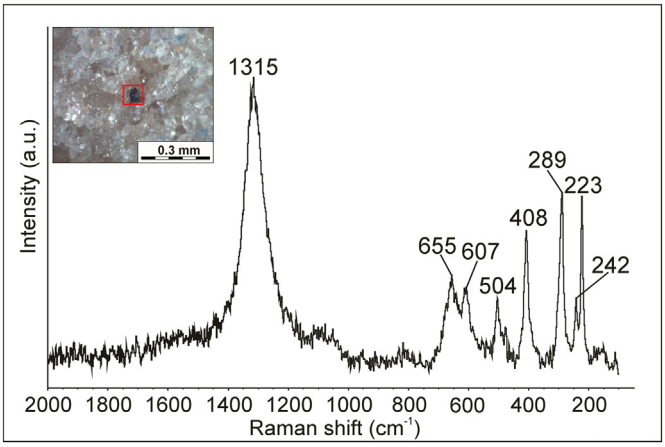

Fig. 10. Raman spectrum of inclusions of hematite within albite.

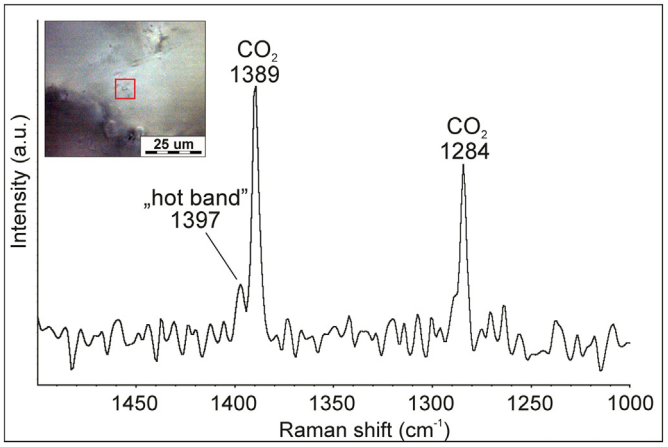

Fig. 12. Raman spectrum of CO_2– bearing fluid inclusions hosted by albite crystals.

4.4. Bulk-rock geochemistry

Whole-rock major and trace element analysis for two varieties of albitites (astrophyllite-poor and -rich ones) as well as associated fenite and granite samples are presented in Table 1. Astrophyllite-devoid albitites are remarkably enriched in Na_2O (~ 11, 16 wt%) and depleted in K_2O (~ 0.27 wt%), MgO (~ 0.03 wt%), CaO (~ 0.07 wt%), and P_2O_5 (>0.01 wt%). The Al_2O and FeO_t contents are ca. 17.59 and 2.97 wt%, respectively. A/NK (0.94–0.95) and A/CNK (0.94) ratios alongside with the presence of normative aegirine at the level of ca. 5 wt% indicate peralkaline character of these rocks (Fig. 15A). Moreover, the samples plot in the alkaline field in the diagram (Fig. 15B). CIA amounts ca 48.5 and plots within the range typical of fresh granites (cf. Nesbitt and Young, 1982). REE patterns of astrophyllite-poor albitites reveal a distinctive V-like shape since they are characterized by moderately fractionated and rightward-inclined LREE segments (La/Sm ratios up to 3.97) accompanied by progressive enrichment in HREE (Gd/Lu ratio up to 0.09) (Fig. 15C). The samples are also marked by pronounced Eu anomaly (Eu/Eu^* ~ 0.29) as well as M-type (concave-downward curves) tetrad effect in the first (La-Nd-related) tetrad, as evidenced by t1 value up to 1.19. Additionally, the W-type tetrad effect (concave-upward curves) in the third (Dy-Ho) tetrad was recognized with t3 values at the level of 0.90. In the primitive diagram (Fig. 15D), astrophyllite-poor albitites exhibit prominent positive Zr-Hf and Nb-Ta anomalies associated with strong depletion in Ba, Sr, and Ti. The main-element composition of astrophyllite-rich albitite is quite similar to astrophyllite-poor samples excluding a predominance of K_2O over Na_2O in the former type. Regarding the trace element distribution, it generally follows the REE pattern observed in astrophyllite-poor albitite since La/Sm, Gd/Lu, and Eu/Eu^* values were calculated as 4.35, 0.19, and 0.28, respectively. Nevertheless, total REE and LILE (including Rb, Ba, Cs) contents appear remarkably high whereas U, Nb, Ta alongside with Sr and Ti are as low as compared with astrophyllite-poor albites. Additionally, tetrad effect is quite poorly developed with t1 and t3 values amounting 1.09 and 0.98 respectively.

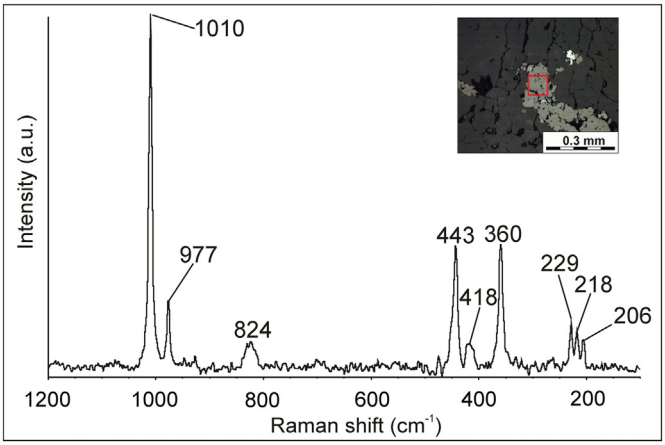

Fig. 11. Raman spectrum of zircon within albitite.

The composition of the fenite slightly resembles those observed in albitites since it is characterized by high Na_2O accompanied by low SiO_2 (64.08 wt%), MgO (0.20 wt%), and P_2O_5 (0.05 wt%) contents. Its LREE pattern is rightward inclined (La/Sm = 5.42) and reveals the presence of strong Eu anomaly (Eu/Eu^* = 0.34). However, fenite differs from albitites with the high CaO (0.69 wt%), MgO (0.20 wt%), and LREE (613.51 ppm) concentrations as well as relatively exhibits flat segments for HREE (Gd/Lu = 0.85) and occurrence of minor negative Ho anomaly. Furthermore, primitive mantle normalized pattern is coherent with those reported for albitites while tetrad effect is considered as negligible with low t1 (1.04) and t2 (0.99) values.

Compared with albitites and fenites, granites have higher contents of SiO_2 (72.69 wt%) and MgO (0.18 wt%) and lower amounts of $Na_2O + K_2O$ (9.7 wt%). Their A/NK and A/CNK values (1.11 and 1.06, respectively) suggest peraluminous affinity whereas high alkalies concentration is typical of alkaline granites. CIA is typical of fresh granites as it amounts 51.55. REE pattern of alkali granite is rightward inclined and show moderate La/Sm (3.93) values, whereas HREE profiles are quite flat (Gd/Lu = 2.46). The sample contain discrete Eu anomaly (Eu/Eu^* = 0.90) and almost no traces of tetrad effect. The abundances of HFSE (Nb, Ta, Zr, and Hf) as well as Sn and Ga are much lower than in albitites and fenites, whereas Rb, Ba, and Sr contents are relatively high. High Zr-Nb-Y-Ce content suggests that granites were derived from A-type magma (Whalen et al., 1987), which was emplaced in post-orogenic settings, as shown by specific Rb/Nb (14.19) and Y/Nb (1.33) ratios (Eby, 1992).

5. Discussion

5.1. Mineralogical and micro-textural implications for the albitite origin

In this paper both primary and secondary origin of albitites from Dmytrivka (SE Ukraine) were considered. According to Kryvdik (2017), see also this study, these rocks share common features with associated fenitized granitoids. This observation makes the strong case for involvement of secondary (hydrothermal-metasomatic) processes during rock formation. However, the results provided by the following research are quite ambiguous and refer to the complex petrogenesis of albitites. The characteristic alignment of albite laths (Fig. 4A–B), which

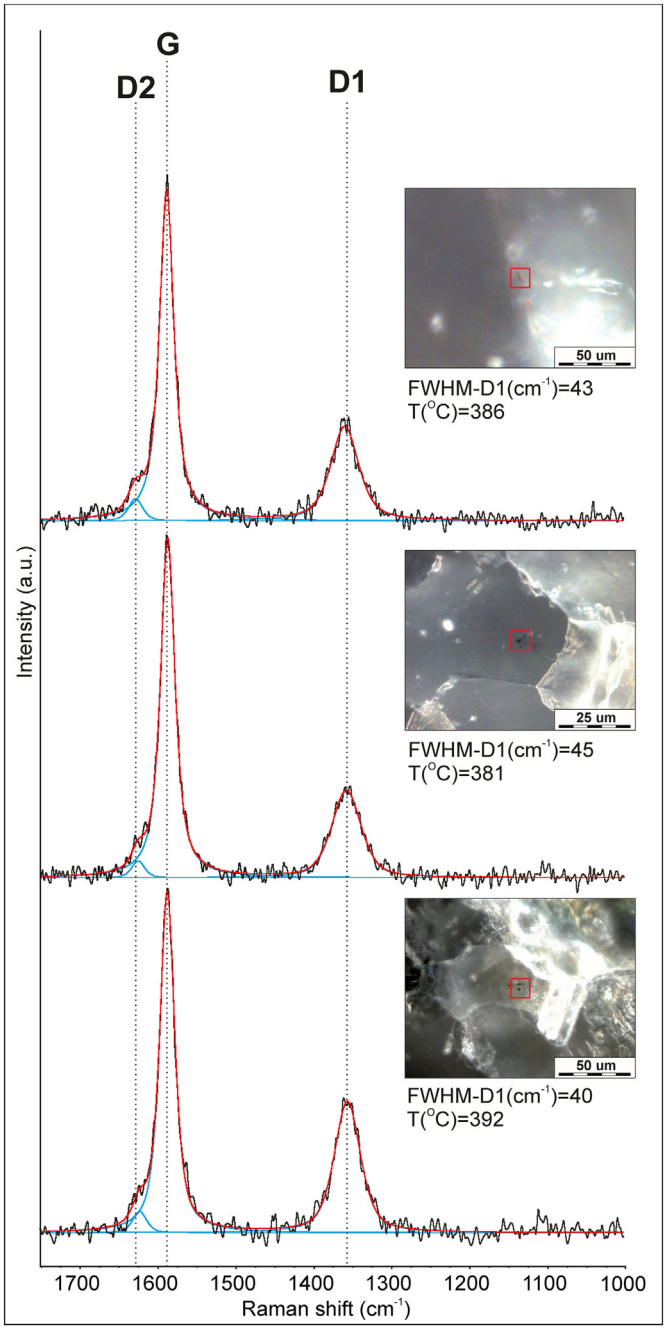

Fig. 13. Example of decomposition of the first order Raman spectra of high-grade CM found as solid inclusions within albite. Note the presence of D2 band occurring as shoulder of the D1 band. D - disordered carbon bands G - graphitic band.

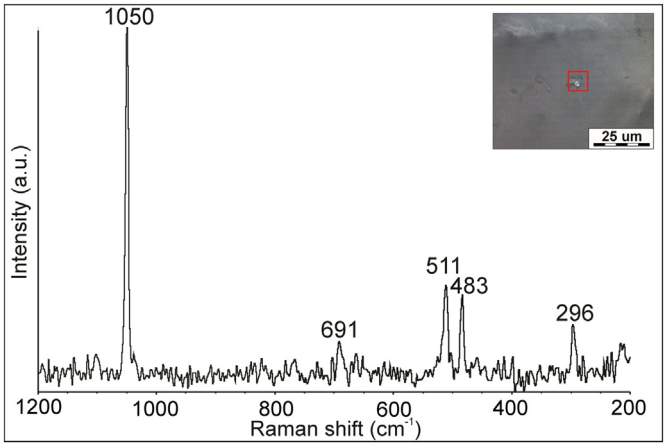

Fig. 14. Raman spectrum of nitrates/sulphates dissolved in fluid inclusions hosted by albite.

could be interpreted as flow texture, as well as snowball appearance caused by Na feldspars laths disseminated through zircon and microcline argue for primary (magmatic) nature of albitites (cf. Huang et al., 2002; Kempe et al., 1999; Lin et al., 1995; Sirqueira et al., 2018). The presence of flow textures indicates intrusive, hypabyssal origin of the rocks emplaced at shallow depths within the crust. Simultaneously, the replacement textures within K-feldspars (e.g. albite rims) are not observed in the rocks. The primary (magmatic) origin is also supported by the presence of zircon-aegirine glomerocrysts since they are typical of magmatic rocks (e.g. Hogan, 1993) and give a clue for magma movement (e.g. convection). The particular zircons and/or aegirine crystals could be welded together (Fig. 4D) as a result of velocity gradient and/or gravitational sorting processes (Condit et al., 2018). Zircon glomerocrysts were absent in alkali-granite and hence could not have been inherited from this rock. Moreover, lack of any F, Cl, Li-bearing phases (topaz, lepidolite) within rock matrix also seems to favour the primary origin of albitites (Haapala, 1997).

On the other hand, there is a strong evidence for contribution of post-magmatic hydrothermal processes during albitites formation, suggesting the rocks have undergone a strong metasomatic overprint related to fenitizing solutions. The occurrence of unzoned pure albite, astrophyllite, and quartz free assemblages in albitites are typical of metasomatic rocks (e.g. Condit et al., 2018; Engvik et al., 2008, 2014; Rubenach and Lewthwaite, 2002). Albite, a common metasomatic product of Na-rich fluids, could be formed here at the expense of K-feldspar or other more An-enriched plagioclase, such as oligoclase (e.g. Saigal et al., 1988). During this reaction some contents of quartz from original rock can be consumed to facilitate the transformation of An-enriched plagioclase or alkali feldspar to more Si-rich albite (Engvik et al., 2008). Moreover, CL observations of albitites show that both albite and alkali feldspar were strongly affected by fluid-rock interaction triggered by migration of fenitizing solutions enriched in Fe^{3+} (Finch and Klein, 1999; Marshall, 1988), which were also responsible for microhematization. The textural appearance of albite crystals without any micro-porosity observed under BSE (Fig. 5A) could be explained by the fact that alteration (fenitization) processes proceeded at relatively high-temperature range conditions, which facilitated annealing of porosity that developed during metasomatic alterations of alkali feldspars (Condit et al., 2018). Such conditions of crystallization are also evidenced by the local development of granoblastic texture (characterized by high angle contacts between albite crystals) that reflects subsolidus textural maturation of albitites and fenites at the elevated temperatures (cf. Suikkanen and Rämö, 2017).

Astrophyllite found in albitite and fenite was possibly formed after alkali amphiboles by metasomatic reactions involving Ti, Nb- and alkaline fluids (Abdel-Rachman, 1992):

3 arfvedsonite +3 water + liquid →2 astrophyllite +8 quartz + free ions + gas.

$3[(K_{0.33}Na_{0.66})Na_2Fe_5Si_8O_{22}(OH,F)] + 3H_2O + K_3Ti_3NbO_{10} \rightarrow 2[(K_2Na)Fe_7(Ti_{1.5}Nb_{0.5})Si_8O_{26}(OH_4,F)] + 8SiO_2 + 6Na^+ + Fe^{2+} + HF + 3O_2$.

The detailed EMPA analyses of astrophyllite from Dmytrivka were presented by Khomenko and Vyshnevskii (2010). Its calculated formulae $(K_{1.75}Rb_{0.01})_{\sum 1.76}(Na_{0.87}Ca_{0.13})_{\sum 1}(Na_{0.07}Fe_{3.78}Mn_{2.64}Mg_{0.24}Zn_{0.15})_{\sum 6.88}(Ti_{1.42}Zr_{0.43}Nb_{0.15})_{\sum 2}(Si_{7.66}Al_{0.36})_{\sum 8.02}O_{26}(OH_4F_{0.94}\square_{0.06})_{\sum 5}$ classifies it is a member of the solid solution between astrophyllite, kupletskite and zircophyllite $Ast_{0.42}Kup_{0.29}Zir_{0.29}$ (Khomenko and Vyshnevskii, 2010). The significant amounts of Zr in astrophyllite structure indicates that metasomatizing alkaline fluids altering arfvedsonite had to be enriched in Zr and Nb, which was probably consumed by newly formed

Table 1
Whole-rock major and trace element analysis of granites, albitites, and fenites.

Sample	Granite	Fenite (after granite)	Astrophyllite-poor albitite		Astrophyllite-rich albitite
Major elements (wt%)					
SiO_2	72.69	64.08	65.06	64.95	64.29
Al_2O_3	13.48	15.35	17.58	17.59	17.71
FeO_t	2.07	5.32	3.31	2.63	1.14
MgO	0.18	0.2	0.04	0.02	0.03
CaO	0.57	0.69	0.08	0.06	0.07
Na_2O	2.93	8.62	11.13	11.18	4.71
K_2O	6.77	3.4	0.36	0.18	9.25
TiO_2	0.17	0.43	0.42	0.8	0.08
P_2O_5	0.05	0.06	<0.01	<0.01	<0.01
MnO	0.04	0.16	0.08	0.07	0.07
Cr_2O_3	0.004	0.006	<0.002	0.003	0.003
Ba	1784	565	142	36	1010
Ni	b.d.l	b.d.l.	<20	<20	<20
Sc	4	5	2	2	<1
LOI	0.7	0.7	0.6	0.5	0.5
Total	99.88	99.11	98.69	97.97	97.95
CIA	51.55	45.36	48.36	48.55	49.84
A/NK	1.11	0.86	0.94	0.95	1
A/CNK	1.06	0.83	0.94	0.94	0.99
Trace elements (ppm)					
Be	<1	15	<1	3	4
Co	1.4	2.3	<0.2	0.4	0.4
Cs	1	1.2	0.2	0.2	3.6
Ga	18.8	77.5	121.9	120.6	67.7
Hf	8.3	112.5	289.4	466.9	342
Nb	13.9	540.5	350.5	536.5	71.7
Rb	197.2	168.9	28.4	11.1	723.4
Sn	<1	23	75	69	17
Sr	217.7	138.3	72.5	91.2	23.1
Ta	0.4	28.8	17.9	28.5	3.4
Th	5.1	21.3	4.3	5.7	16.9
U	1.2	4.2	0.8	1.5	0.4
V	<8	14	<8	<8	13
W	0.6	0.8	2.1	3.4	<0.5
Zr	328.7	4654.6	8777.3	13,895	13,979.6
Y	18.5	65.6	29.1	32.9	102.1
La	36	152.3	14.5	16.9	66.1
Ce	71.3	291.5	35.6	43.6	142.2
Pr	8.35	31.05	3.99	4.75	16.2
Nd	31.4	105.2	13.7	16.6	56.3
Sm	5.72	17.55	2.29	2.66	9.49
Eu	1.53	1.81	0.25	0.25	0.98
Gd	4.57	14.1	2.07	2.27	9.32
Tb	0.66	2.24	0.43	0.49	2.09
Dy	3.76	13.3	4.38	4.99	18.11
Ho	0.71	2.64	1.37	1.62	5.2
Er	1.93	8.43	7.15	8.04	22.62
Tm	0.27	1.45	1.5	1.82	4.44
Yb	1.51	11.02	13.64	16.71	36.05
Lu	0.23	2.04	2.7	3.34	6
REE sum	167.94	654.63	103.57	124.04	395.10
LREE/HREE	17.52	17.52	2.32	2.35	3.18
K/Rb	142.50	83.56	52.62	67.31	53.07
La/Sm	3.93	5.42	3.95	3.97	4.35
La/Yb	16.20	9.39	0.72	0.69	1.25
Gd/Lu	2.46	0.85	0.09	0.08	1.19
Eu/Eu^*	0.90	0.34	0.31	0.27	0.28
t1	1.00	1.04	1.17	1.19	1.09
t3	0.97	0.99	0.90	0.90	0.98
t4	0.95	0.96	1.02	1.06	1.08
$TE_{1.3}$	0.98	1.01	1.03	1.03	1.03

Note: CIA - chemical index of alteration [molar $Al_2O_3/(Na_2O + K_2O + Al_2O_3 + CaO)$]; A/NK - molar $Al_2O_3/(Na_2O + K_2O)$; A/CNK -molar $Al_2O_3/(CaO + Na_2O + K_2O)$; Eu/Eu^* - calculated after Lawrence et al. (2006); degree of tetrad effect in the first (t1), third (t3), and fourth (t4) tetrad, as well as its total value ($T_{1,3}$) were calculated after Irber (1999).

astrophyllite instead of crystallization of new generation of zircon crystals of hydrothermal genesis.

Fenitizing fluids are also the most probably responsible for transformation of alkali amphiboles (main components of fenites) into sodium rich pyroxenes, found within both fenites and albitites (cf. Martin and Morgan, 1988; Rubie and Gunter, 1983), and are not ubiquitously present in alkaline granite. As reported by e.g. Marks et al. (2003) and Bonin (1982), the formation of aegirine at the expense of arfvedsonite requires highly- oxidizing conditions and hence could be expressed by the following reaction:

$$Na_3Fe_5Si_8O_{22}(OH_2) + O_2 \rightarrow 3NaFeSi_2O_6 + Fe_2O_3 + SiO_2 + H_2O$$

It is also probable that aegirine could had replaced quartz in fenites and albitites by the reaction:

$$2H_2O + Na^+ + Fe^{3+} + 2SiO_2\ (aq) = 4H + + NaFeSi_2O_6$$

(Rubie and Gunter, 1983)

However, no appropriate textural evidence can be provided in the following study. Furthermore, biotite (representing the main mafic component of alkali granite) was converted into alkali-amphibole (cf. Sindern and Kramm, 2000). However, arfvedsonite/riebeckite could also crystallize directly from melt during late stage of magma evolution since they are interstitial to feldspars.

Zircon is one of a few minerals, which may survive the influx of fluids and hence preserves the fluid history of the rock (Curtis, 2017). Nevertheless, strongly alkaline solutions may easily trigger off its dissolution (Rubatto et al., 2008). Although zircon glomerocrysts found within albitite were previously interpreted as magmatic, they also carry the signature typical of metasomatic alteration. Firstly, the particular zircon crystals exhibit characteristic patchy zoning (Fig. 5C–D), which is typical for fluid-mineral interactions (e.g. Tomaschek, 2003; Xie et al., 2005) whereas Geisler et al. (2007) attributed the origin of this texture to the dissolution-recrystallization process. Similarly, strong fracturing coupled with secondary porosity of zircon grains indicate they might be overprinted by strong deuteric alteration (Yang et al., 2014). Additionally, the presence of domains with two various CL colours producing various CL spectra also confirm that various regions of zircons differ in origin between each other (Dumańska-Słowik et al., 2011). The regions with dark navy blue CL colours, characterized by higher degree of crystallinity (distinct emission line at 368 nm owing to perfect crystal lattice) are the most probably recrystallized regions of zircon (Nasdala et al., 2003). Furthermore, zircon glomerocrysts occur only in albitites (not found in alkali granite and fenite), suggesting this texture could be related to deformation of single zircon grains, during fluid flow and alteration (Condit et al., 2018). The recorded Raman spectrum of zircon from albitite can be both typical of mineral formed under magmatic or hydrothermal origin (Yang et al., 2014), however the other textural characteristic (slight oscillatory zonation, distinct patchy zoning, porosity and fracturing) undoubtedly indicates its high-temperature magmatic genesis.

Albite, main component of albitites from Dmytivka contains some solid and fluid inclusions. Solid inclusions are represented by rutile, hematite and carbonaceous matter. Rutile and hematite could be probably formed during fenitization and albitization, as a by-product of reaction: Ilmenite → Rutile + Hematite (Engvik et al., 2008). Whereas, the origin of carbonaceous substance hosted by albite seems to be quite vague; derived from magma (e.g. Florovskaya et al., 1968; Nivin, 2002) or trapped from the surrounding rocks (e.g. Fersman, 1931). Pripachkin et al. (1985) documented the presence of bitumens and methane inclusions of secondary origin in various rocks of alkaline Khibina Massif, which could provide the existence of late C-H- rich fluids at the very late stage of subsolidus re-equilibration (Barkov et al., 2000). Chukanov et al. (2009) noted that during post-magmatic activity the mineralization of Ti, Nb, Zr-rich phases was directly preceded by sedimentation of carbonaceous matter. All these high-valent transition elements were activated during metasomatic alterations in the Oktiabrski complex (Dumańska-Słowik, 2016). Assuming the secondary origin of CM found within albitite, the temperatures calculated using FWHM of D1 band reflect the character of metasomatizng (fenitizing) solutions,

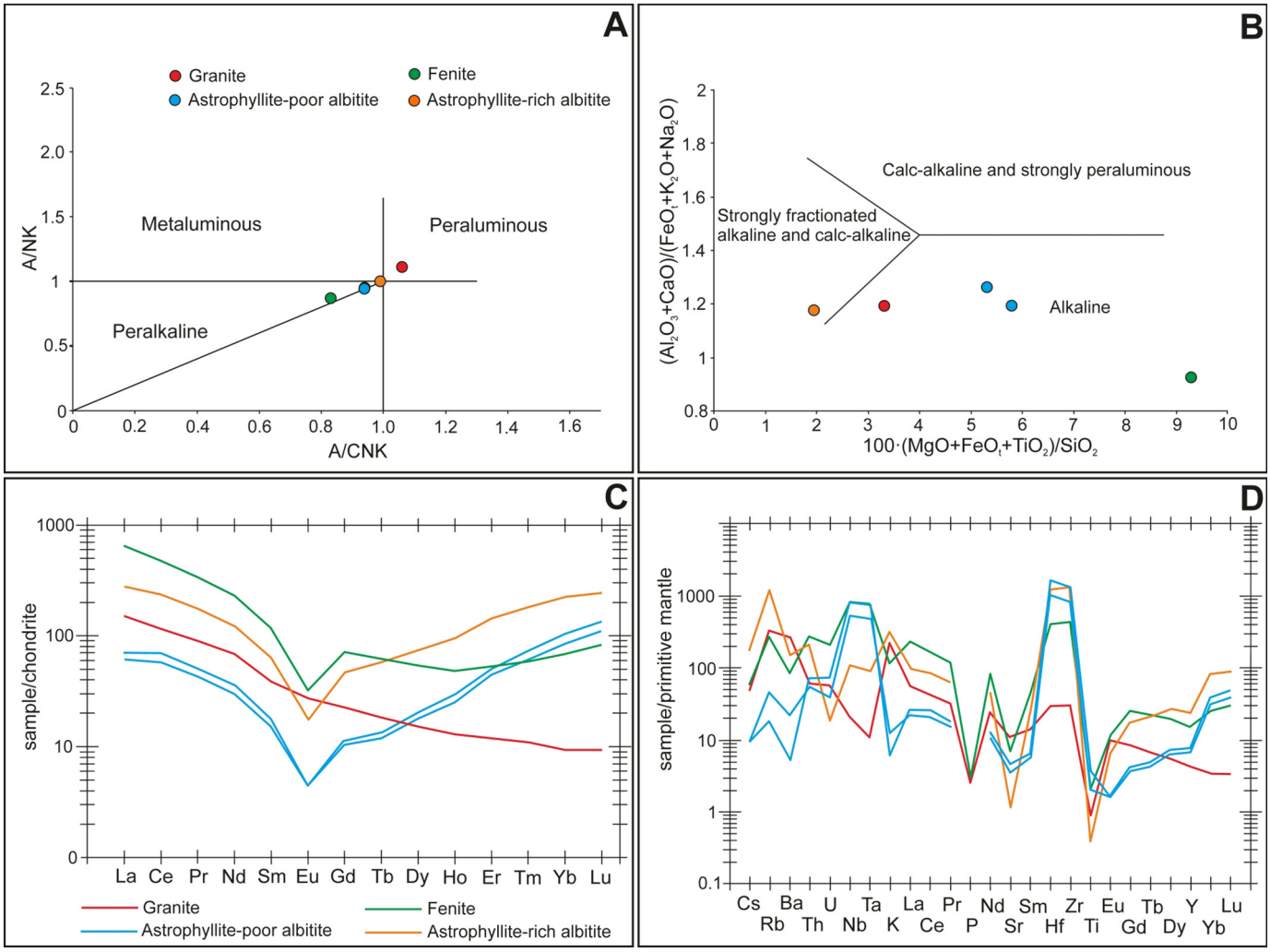

Fig. 15. (A,B) The distribution of granite, fenite, and albitite within A/CNK versus A/NK (molar) diagram (A) and $(Al_2O_3 + CaO)/(FeO_t + Na_2O + K_2O)$ vs. $100\cdot(MgO + FeO_t + TiO_2)/SiO_2$ plot (B); Diagrams are after Maniar and Piccoli (1989) and Sylvester (1989), respectively; (C, D) Chondrite normalized REE patterns (C) and multi-element spider diagrams (D) for granite, albitite, and fenite samples. Normalization values are from McDonough and Sun (1995).

which undoubtedly affected both fenites and albitites. The calculated temperatures of 381 °C–392 °C (Fig. 13) seem to be consistent with micro-textural and CL observations suggesting relatively high-temperature alterations. Moreover, the lack of any carbonates in albitites from Dmytrivka together with the presence of carbonaceous matter indicates rather low activity of oxygen in the moment of its formation (Chukanov et al., 2009).

Fluid inclusions found in secondary albite contain mainly CO_2, which is a common component of fluids in the deep crust, where alkali granites and probably albitite from the Oktiabrski complex were formed and emplaced. Van der Kerkhof and Thiéry (2001) noted that carbonic fluids in magmatic rocks resulted from oxidation of organic matter or as a product of decarbonization in calc-silicate and carbonaceous rocks. The occurrence of inclusions of both carbonaceous substance and CO_2 in albite crystals could support that CO_2, might originate from bituminous substance. Some fluid inclusions contain also sulphates (or nitrates?), which could be also the components of metasomatizing fluids.

5.2. Constraints from bulk-rock chemistry

According to so-called isocon diagrams (Fig. 16), which show behaviour of particular elements during alteration processes, granite-fenite transition is characterized by significant increase in Na_2O, FeO_t and slight impoverishment in Al_2O_3, TiO_2 and CaO. Otherwise, SiO_2 and K_2O contents decrease in fenites, while MgO remains nearly constant in both types of rocks. Regarding trace elements, almost all of them (in particular REE and HFSE) note the abrupt increase in fenites whereas LILE concentrations (including Rb, Sr, Ba) are lower than in alkali-granites. Not only do the aforementioned changes reflect alteration of K-feldspar into albite, but are related to highly-oxidizing and high-temperature, fenitizing solutions responsible for i.e. LREE- enrichment and leaching of LILE (cf. Kopecký Jr. et al., 1997; Morogan, 1989; Robins and Tysseland, 1979). Higher HFSE contents in fenite should be in turn ascribed to the presence of accessory phases including e.g. astrophyllite and zircon, as well as alkali-pyroxenes and amphiboles (Eby, 1975; Morogan, 1989). Despite the fact that albities seem to be of primary origin, we put their chemical composition into isocon diagram to better illustrate the differences in chemical composition between albites-fenites and albitites-alkali-granites. As it was shown in the Fig. 16, astrophyllite-poor albitites are marked by increase in Na_2O, Al_2O_3, FeO_t, and TiO_2 coupled with decrease of MgO, CaO, K_2O, and SiO_2 relative to alkali-granites. They are depleted in LILE (including Cs, Rb, Ba, Sr) compared to alkali-granites, while Nb, Ta Zr, Hf, Ga, and Sn contents exhibit progressive enrichment. These changes possibly reflect both crystallization processes from granitic melt as well as post-magmatic alterations. Additionally, the occurrence of

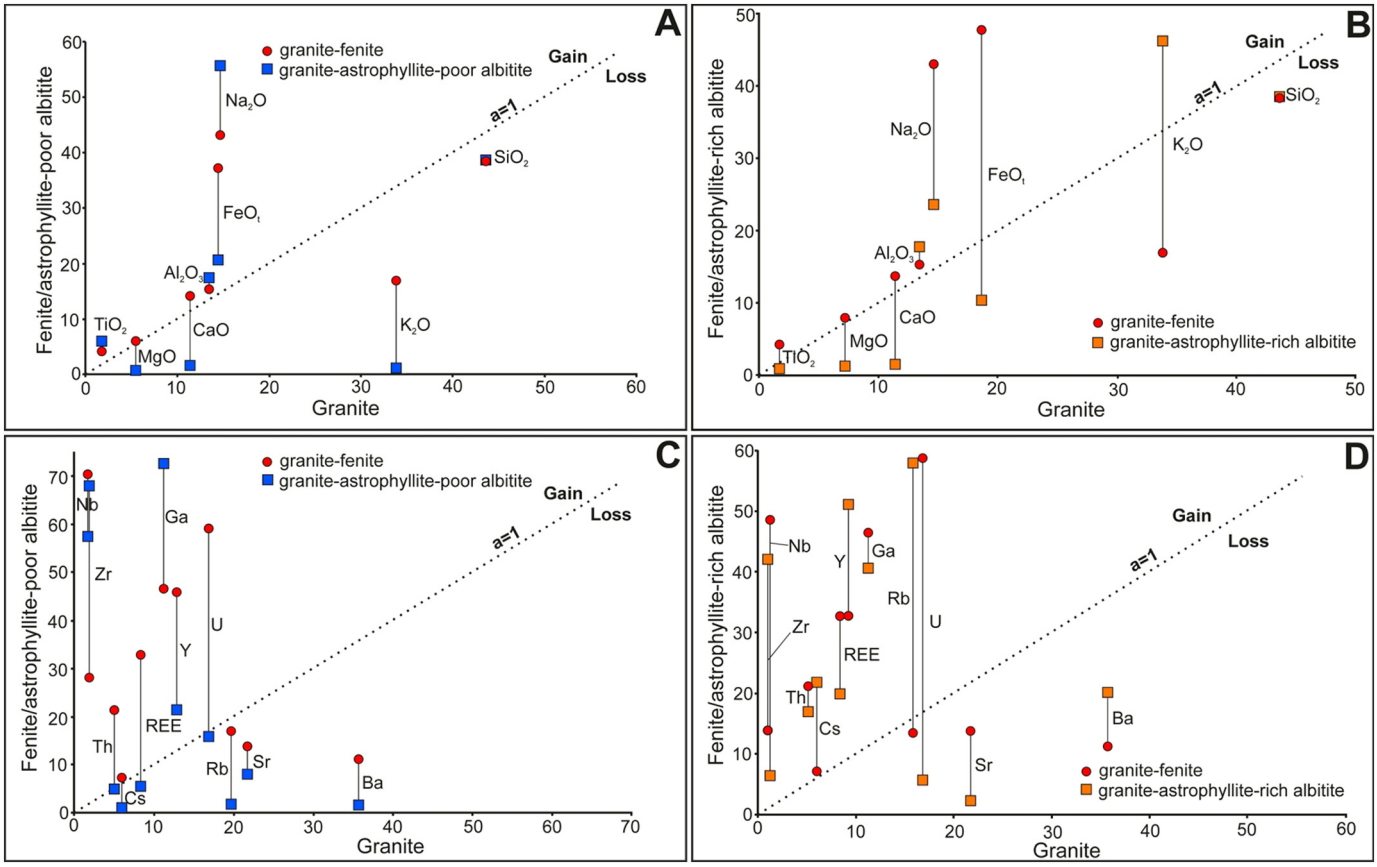

Fig. 16. Isocon diagrams showing relative gain and lose of main (A, C) and trace (B, D) elements during fenitization; Chemical constituents gained during alteration (fenitization) plot above a = 1 dashed line whereas those found below these line show depletion relative to alkali-granites; The data for albitites, which formed during magmatic processes but were subsequently altered during fenitization, were given for comparison. Note the scaling factors were added to some of elements.

astrophyllite in albitite resulted in increasing LILE (especially K and Rb) contents in whole-rock analysis.

Albitites (especially astrophyllite-poor variety) exhibit M-type tetrad effect in the first (La-Sm) tetrad combined with inversion of REE patterns (negative LREE and positive HREE segments) and low K/Rb ratios (52.62–67.31). What is more, the M-type effect in the first tetrad is coupled with W-type effect in the third tetrad. Overall, the phenomenon of tetrad effect was reported from highly-evolved granitic rocks (McLennan, 1994; Bau, 1996, 1997; Pan, 1997;) and could be assigned to the interactions between aqueous fluids and melt during late stages of alkali-granite evolution (Clarke, 1992; Irber, 1999; Zhenhua et al., 2002). The coupled M- an W-type tetrad effect, which was not frequently described from granitoids and associated rocks, provides an evidence that albitites were imposed by Si, K, Al-bearing high-temperature hydrothermal fluids (El-Mezayen et al., 2015; Zhao et al., 2010). The Eu anomaly found within albitites have possibly originated from accumulation of accessory phases (zircon and pyrochlore) within rock matrix and corresponding fractionation in the melt-fluid system (Muecke and Clarke, 1981). Consequently, the role of pre-crystallization plagioclase fractionation in progressive depletion of Eu should be ignored. Otherwise, the nature of Eu anomaly in fenites demands further investigations, but it may be connoted with reducting conditions of crystallization and Eu depletion in accessory phases, such as zircon and astrophyllite.

6. Conclusions

On the basis of mineralogical, textural, and geochemical characteristics, a distinctive magmatic-hydrothermal origin of albitites of Dmytrivka quarry has been favourably adopted. The possible scenario proposed in this study assumes that they were emplaced as highly differentiated volatile-rich A-type magma at shallow depths of the crust. This idea is evidenced by: (1) subparallel alignment of albite laths (flow texture), (2) snowball texture (albite laths enclosed in zircon and microcline), (3) the presence of glomerocrysts made of zircon-aegirine assemblages. Moreover, the geochemical features prove there are no clear gradual changes in chemical composition of albitites and fenites, as it would be expected on the assumption that albitites could represent the most advanced stage of fenitization of host granitoids. However, albitites carry the signature of strong metasomatic overprint triggered by high-temperature and highly-oxidizing alkaline-bearing solutions as shown by: (1) high-angle contacts between albite crystals (polygonal texture), (2) Fe^{3+}-activated red luminescence of albite and K-feldspar, (3) lack of quartz, (4) occurrence of astrophyllite as major hydrothermal-metasomatic phase, (5) general mineral similarities between albitites and associated fenites, (6) micro-textural features of zircon (variations of CL colours, spongy appearance, and secondary micro-porosity). The alterations have possibly contributed to increase of HFSE (i.e. Nb, Ta, Zr) in both fenites and albitites. Additionally, the composite W- and M- type REE tetrad effect also invokes a complex origin of albitites, which was related to both melt-aqueous phases interactions and subsequent Si, K, Al high-temperature fluid action.

Acknowledgements

The contribution from Leszek Giro and Tomasz Toboła for assistance in performing SEM-CL and Raman spectroscopy analyses, respectively.

We would like to thank the reviewers, Prof. Janina Wiszniewska and Prof. Franco Pirajno for their useful and friendly comments, which helped to improve the manuscript. The work was financially supported by AGH the University of Science and Technology, the research project no 11.11.140.158.

References

Abdel-Rachman, A.M., 1992. Mineral chemistry and paragenesis of astrophyllite from Egypt. Mineralogical Magazine 56, 17–26.

Agakhanov, A.A., Pautov, L.A., Sokolova, E., Abdu, Y.A., Karpenko, V.Y., 2016. Two astrophyllite-supergroup minerals: bulgakite, a new mineral from the Darai-Pioz alkaline massif, Tajikistan and revision of the crystal structure and chemical formula of nalivkinite. The Canadian Mineralogist 54, 33–48.

Arakawa, M., Yamamoto, J., Kagi, H., 2007. Developing micro-Raman mass spectrometry for measuring carbon isotopic composition of carbon dioxide. Applied Spectroscopy 61 (7), 701–705.

Azer, M.K., Stern, R.J., Kimura, J.I., 2010. Origin of a late Neoproterozoic (605±13 Ma) intrusive carbonate–albitite complex in Southern Sinai, Egypt. International Journal of Earth Sciences (Geol Rundsch) 99, 245–267.

Barkov, A.Y., Martin, R.F., Men'shikov, Y.P., Savchenko, Y.E., Thibault, Y., Laajoki, K.V.O., 2000. Edgarite, $FeNb_3S_6$, first natural niobium-rich sulphide from the Khibina alkaline complex, Russian Far North: evidence for chalcophile behavior of Nb in a fenite. Contributions to Mineralogy and Petrology 138, 229–236.

Bau, M., 1996. Controls on the fractionation of isovalent trace elements in magmatic and aqueous systems: evidence from Y/Ho, Zr/Hf, and lanthanide tetrad effect. Contributions to Mineralogy and Petrology 123, 323–333.

Bau, M., 1997. The lanthanide tetrad effect in highly evolved felsic igneous rocks—a reply to the comment by Y. Pan. Contributions to Mineralogy and Petrology 128, 409–441.

Beyssac, O., Goffé, B., Chopin, C., Rouzaud, J., 2002. Raman spectra of carbonaceous material in 772 metasediments: a new geothermometer. Journal of Metamorphic Geology 20 (9), 859–871. https://doi.org/10.1046/j.1525-1314.2002.00408.x.

Beyssac, O., Goffé, B., Petitet, J.P., Froigneux, E., Moreau, M., Rouzaud, J.N., 2003. On the characterization of disordered and heterogeneous carbonaceous materials by Raman spectroscopy. Spectrochimica Acta Part A: Molecular and Biomolecular Spectroscopy 59, 2267–2276. https://doi.org/10.1016/S1386-1425(03)00070-2.

Blanc, P., Baumer, A., Cesbron, F., Ohnenstetter, D., Panczer, G., Remond, G., 2000. Systematic cathodoluminescence spectral analysis of synthetic doped minerals. In: Pagel, M., Barbin, V., Blanc, P., Ohnenstetter, D. (Eds.), Cathodoluminescence in Geosciences, pp. 127–160.

Bonin, B., 1982. Les granites des complexes annulaires (B.R.G.M. Manuels et Méthodes. 4).

Burke, E.A.J., 2001. Raman microspectrometry of fluid inclusions. Lithos 55, 139–158.

Cámara, F., Gagne, O.C., Belakovskiy, D.I., 2017. New minerals names. American Mineralogist 102, 1143–1148.

Castorina, F., Masi, U., Padalino, G., Palomba, M., 2006. Constraints from geochemistry and Sr-Nd isotopes for the origin of albitite deposits from Central Sardinia (Italy). Mineralium Deposita 41, 323–338.

Cathelineau, M., 1988. Accessory mineral alteration in peraluminous granites at the hydrothermal stage: a review. Rendiconti della Societa Italiana di Mineralogia e Petrologia 43, 499–508.

Chukanov, N.V., Ermolaeva, V.N., Pekov, I.V., Lahti, S., 2009. Carbonaceous matters in pegmatites of different genetic types and their role in formation of mineral associations. New Data on Minerals. M. 44, 11–23.

Clarke, D.B., 1992. The mineralogy of peraluminous granites: a review. The Canadian Mineralogist 19, 3–17.

Condit, C.B., Mahan, K.H., Curtis, K.C., Möller, A., 2018. Dating metasomatism: monazite and zircon growth during amphibolite facies albitization. Minerals 8, 187.

Curtis, K., 2017. Using Zircon Morphology to Understand Metasomatic Fluid Alteration during the Big Sky Orogeny. Undegraduate Honors Theses 1509. https://scholar.colorado.edu/honr_theses/1509.

Donskoy, A.N., 1982. The Nepheline Complex of Alkaline Oktyabrski Massif. The Ukrainian Academy of Science, Kiev (in Ukrainian).

Dumańska-Słowik, M., 2016. Evolution of mariupolite (nepheline syenite) in the alkaline Oktiabrski Massif (Ukraine) as the host of potential Nb–Zr–REE mineralization. Ore Geology Reviews 78, 1–13.

Dumańska-Słowik, M., Sikorska, M., Heflik, W., 2011. Dissolved-recrystallized zircon from mariupolite in the Mariupol Massif, Priazovje (SE Ukraine). Acta Geologica Polonica 61 (3), 277–288.

Eby, G.N., 1975. Abundance and distribution of the rare-earth elements and yttrium in the rocks and minerals of the Oka carbonatite complex, Quebec. Geochimica et Cosmochimica Acta 39 (5), 597–620.

Eby, G.N., 1992. Chemical subdivision of the A-type granitoids: petrogenetic and tectonic implications. Geology 20, 641–644.

El-Mezayen, A.M., El-Feky, M.G., Omar, S.A., Ibrahim, S.A.E.A., 2015. Geochemistry and a composite M-type with W-type of REE tetrad effect in altered granites of Abu Furad area, Central Eastern Desert, Egypt. Greener Journal of Geology and Earth Sciences 3, 13–29. https://doi.org/10.15580/GJGES.2015.2.111915161.

Engvik, A.K., Putnis, A., FitzGerald, J., Austrheim, H., 2008. Albitization of granitic rocks: the mechanism of replacement of oligoclase by albite. The Canadian Mineralogist 46, 1401–1415.

Engvik, A.E., Ihlen, P.M., Austrheim, H., 2014. Characterisation of Na-metasomatism in the Sveconorwegian Bamble Sector of South Norway. Geoscience Frontiers 5, 659–672.

Escribano, R., Sloan, J.J., Siddique, N., Sze, N., Dudev, T., 2001. Raman spectroscopy of carbon containing particles. Vibrational Spectroscopy 26, 179–186.

Fermi, E., 1931. Über den Ramaneffekt des Kohlendioxyds. Zeitschrift für Physik 71, 250–259.

Ferrari, A.C., Robertson, J., 2000. Interpretation of Raman spectra of disordered and amorphous carbon. Physical Review B 61, 95–107.

Fersman, A.E., 1931. Pegmatites, their Scientific and Practical Importance. V. 1. Granitic Pegmatites. L.: AN SSSR (In Russian).

Finch, A.A., Klein, J., 1999. The causes and petrological significance of cathodoluminescence emission from alkali feldspars. Contributions to Mineralogy and Petrology 135, 234–243.

Florovskaya, V.N., Zezin, R.B., Ovchinnikova, L.I., Pikovskii, Yu.I., Teplitskaya, T.A., 1968. Diagnostics of Organic Matters in Rocks and Minerals of Magmatic and Hydrothermal Origin. Nauka, Moscow (In Russian).

Frezzotti, M.L., Tecce, F., Casagli, A., 2012. Raman spectroscopy for fluid inclusion analysis. Journal of Geochemical Exploration 112, 1–20.

Gaft, M., Reisfeld, R., Panczer, G., 2005. Luminescence Spectroscopy of Minerals and Materials. Berlin. Heidelberg. Springer-Verlagv, New York.

Geisler, T., Schaltegger, U., Tomaschek, F., 2007. Reequilibration of zircon in aqueous fluids and melts. Elements 3 (1), 43–50.

Gorobets, B.S., Rogojine, A.A., 2002. Luminescent Spectra of Minerals. Moscow.

Götze, J., 2000. Cathodoluminescence Microscopy and Spectroscopy in Applied Mineralogy (Freiberg).

Haapala, I., 1997. Magmatic and postmagmatic processes in tin-mineralized granites: topaz-bearing leucogranite in the Eurajoki rapakivi granite stock, Finland. Journal of Petrology 38, 1645–1659.

Hogan, J.P., 1993. Monomineralic glomerocrysts: Textural evidence for mineral resorption during crystallization of igneous rocks. The Journal of Geology 101 (4), 531–540.

Huang, X.L., Wang, R.C., Chen, X.M., Hu, H., Liu, C.S., 2002. Vertical variations in the mineralogy of the Yichun topaz–lepidolite granite, Jiangxi Province, southern China. The Canadian Mineralogist 40 (4), 1047–1068.

Irber, W., 1999. The lanthanide tetrad effect and its correlation with K/Rb, Eu/Eu*, Sr/Eu, Y/Ho, and Zr/Hf of evolving peraluminous granite suites. Geochimica et Cosmochimica Acta 63 (3–4), 489–508.

Johnson, C.A., Harlow, G.E., 1999. Guatemala jadeitites and albitites were formed by deuterium-rich serpentinizing fluids deep within a subduction zone. Geology 27, 629–632.

Kampf, A.R., Rossman, G.R., Steele, I.M., Pluth, J.J., Dunning, G.E., Walstrom, R., 2010. Devitoite, a new heterophyllosilicate mineral with astrophyllite-like layers from eastern Fresno County, California. The Canadian Mineralogist 48, 29–40.

Kayama, M., Nakano, S., Nishido, H., 2010. Characteristics of emission centers in alkali feldspar: a new approach by using cathodoluminescence spectral deconvolution. American Mineralogist 95, 1783–1795.

Kempe, U., Goetze, J., Dandar, S., Habermann, D., 1999. Magmatic and metasomatic processes during formation of the Nb-Zr-REE deposits Khaldzan Buregte and Tsakhir (Mongolian Altai): indications from a combined CL-SEM study. Mineralogical Magazine 63 (2), 165–177.

Khomenko, V., Vyshnevskii, O., 2010. Astrophyllite from Alkaline Metasomatized Rocks (Dmytrivka, Azov region): Crystal Chemistry, Spectroscopy, Inclusions. Alkaline Rocks: Petrology, Mineralogy, Geochemistry. Proceedings of conference, 19-21.09.2010. Semeneneko Institute of Geochemistry, Mineralogy and Ore Formations, Kiev, pp. 34–35.

Kopecký Jr., L., Chlupáčová, M., Klomínský, J., Sokol, A., 1997. The Čistá-Jesenice pluton in western Bohemia: geochemistry, geology, petrophysics and ore potential. Sbor. geol. Věd, ložisk. Geol. Mineral 31, 97–127.

Kouketsu, Y., Mizukami, T., Mori, H., Endo, S., Aoya, M., Hara, H., Nakamura, D., Wallis, S., 2014. A new approach to develop the Raman carbonaceous material geothermometer for low-grade metamorphism using peak width. Island Arc 23, 33–50.

Kryvdik, S., 2017. Apofenitic albitites of Ukrainian Shield. Heokhimiya ta rudoutvorennya. 38, 58–69 (in Ukrainian).

Lawrence, M.G., Greig, A., Collerson, K.D., Kamber, B.S., 2006. Rare earth element and yttrium variability in South East Queensland waterways. Aquatic Geochemistry 12, 39–72.

Legodi, M.A., De Waal, D., 2006. The preparation of magnetite, goethite, hematite and maghemite of pigment quality from mill scale iron waste. Dyes and Pigments 74, 161–168.

Lin, Y., Pollard, P.J., Hu, S., Taylor, R.G., 1995. Geologic and geochemical characteristics of the Yichun Ta-Nb-Li deposit, Jiangxi Province, South China. Economic Geology 90, 577–585.

Maniar, P.D., Piccoli, P.M., 1989. Tectonic discrimination of granitoids. Geological Society of America Bulletin 101, 635–643.

Marks, M., Vennemann, T., Siebel, W., Markl, G., 2003. Quantification of magmatic and hydrothermal processes in a peralkaline syenite–alkali granite complex based on textures, phase equilibria, and stable and radiogenic isotopes. Journal of Petrology 44 (7), 1247–1280.

Marshall, D.J., 1988. Cathodoluminescence of Geological Materials. Boston.

Marshall, C.P., Marshall, A.O., 2013. Raman hyperspectral imaging of microfossils: potential pitfalls. Astrobiology 13 (10), 920–931.

Martin, R.F., Morgan, V., 1988. Partial melting of fenitized crustal xenoliths in the Oldoinyo Lengai carbonatitic volcano., Tanzania: Reply. American Mineralogist 73, 1468–1471.

McDonough, W.F., Sun, S.S., 1995. The composition of the Earth. Chemical Geology 120, 223–253.

McKeown, D.A., 2005. Raman spectroscopy and vibrational analyses of albite: from 25 °C through the melting temperature. American Mineralogist 90, 1506–1517.

McLennan, S.M., 1994. Rare earth element geochemistry and the "tetrad" effect. Geochimica et Cosmochimica Acta 58, 2025–2033.
Mohammad, Y., Maekawa, H., Lawa, F.A., 2007. Mineralogy and origin of Mlakawa albitite from Kurdistan region, northeastern Iraq. Geosphere 3 (6), 624–645.
Morogan, V., 1989. Mass transfer and REE mobility during fenitization at Alnö, Sweden. Contributions to Mineralogy and Petrology 103 (1), 25–34.
Muecke, G.K., Clarke, D.B., 1981. Geochemical evolution of the South Mountain Batholith, Nova Scotia: rare-earth element evidence. The Canadian Mineralogist 19, 133–145.
Nasdala, L., Zhang, M., Kempe, U., Panczer, G., Gaft, M., Andrut, M., Plötze, M., Hoskin, P., 2003. Spectroscopic methodsapplied to zircon. In: Hanchar, J. (Ed.), Zircon, Rev Mineral Geochem. vol. 53, pp. 427–466.
Nesbitt, H.W., Young, G.M., 1982. Early Proterozoic climates and plate motions inferred from major element chemistry of lutites. Nature 299, 715–717.
Nivin, V.A., 2002. Gas saturation of minerals in connection with the problem of origin of hydrocarbon gases in the rocks of the Khibinsky and Lovozersky alkaline massifs. Geokhimiya 9, 976–992 (in Russian).
Palomba, M., 2001. Geological, mineralogical, geochemical features and genesis of the albitite deposits of Central Sardinia (Italy). Rendiconti Seminario Facoltà Scienze Università Cagliari Supplemento 71 (2), 35–57.
Pan, Y., 1997. Controls on the fractionation of isovalent trace elements in magmatic and aqueous systems: evidence from Y/Ho, Zr/Hf, and lanthanide tetrad effect—A discussion of the article by M. Bau. Contributions to Mineralogy and Petrology 128, 405–408.
Pin, C., Monchoux, P., Paquette, J.L., Azambre, B., Wang, R.C., Martin, R.F., 2006. Igneous albitite dikes in orogenic lherzolites, western Pyrénées, France: a possible source for corundum and alkali feldspar xenocrysts in basaltic terranes.II. Geochemical and petrogenetic considerations. The Canadian Mineralogist 44, 843–856.
Ponomarenko, A.N., Krivdik, S.G., Grinchenko, A.V., 2013. Alkaline rocks of the Ukrainian Shield: some mineralogical, petrological and geochemical features. Mineralogia 44 (3–4), 115–124.
Pripachkin, V.A., Pavlova, M.A., Galakhova, T.N., Volokhova, T.S., Malashkina, V.T., 1985. Bitumen of the Khibina carbonatites (in Russian). Doklady Akademii Nauk SSSR 281, 1424–1426.
Robins, B., Tysseland, M., 1979. Fenitization of some mafic igneous rocks in the Seiland province, northern Norway. Norsk Geologisk Tidsskrift 59 (1), 1–23.
Rosso, K.M., Bodnar, R.J., 1995. Microthermometric and Raman spectroscopic detection limits of CO_2 in fluid inclusions and the Raman spectroscopic characterization of CO_2. Geochimica et Cosmochimica Acta 59, 3961–3975.
Rubatto, D., Müntener, O., Barhoorn, A., Gregory, C., 2008. Dissolution–reprecipitation of zircon at low-temperature, high-pressure conditions (Lanzo Massif; Italy). American Mineralogist 93, 1519–1529.
Rubenach, M.J., Lewthwaite, K.A., 2002. Metasomatic albitites and related biotite-rich schists from a low-pressure polymetamorphic terrane, Snake Creek Anticline, Mount Isa Inlier, North-Eastern Australia: Microstructures and P-T-d paths. Journal of Metamorphic Geology 20, 191–202.
Rubie, D.C., Gunter, W.D., 1983. The role of speciation in alkaline igneous fluids during fenite metasomatism. Contributions to Mineralogy and Petrology 82 (2–3), 165–175.
Saigal, G.C., Morad, S., Bjørlykke, K., Egeberg, P.K., Aagaard, P., 1988. Diagenetic albitization of detrital K-feldspar in Jurassic, Lower Cretaceous, and Tertiary clastic reservoir rocks from offshore Norway. I. Texture sand origin. Journal of Sedimentary Petrology 58, 1003–1013.
Schwartz, M.O., 1992. Geochemical criteria for distinguishing magmatic and metasomatic albite-enrichment in granitoids: examples from Ta-Li granite Yivhun (China) and the Sn-W deposit Tikus (Indonesia). Mineralium Deposita 27, 101–108.
Shumlyanskyy, L.V., Ponomarenko, O.M., Stepanyuk, L.M., Cuney, M., Petrenko, O.V., 2015. Albitite-hosted U deposits in the central part of the Ukrainian shield: a mantle-plume source of the ore-forming fluids? Conference paper, technical meeting on uranium deposits formed in the gondwana supercontinent. The Importance of the Gondwana, Karoo, Paraná and Similar Sedimentary Basins At: IAEA Headquarters, Vienna, Austria https://www.researchgate.net/publication/279406296_Albitite-hosted_U_deposits_in_the_central_part_of_the_Ukrainian_shield_a_mantle-plume_source_of_the_ore-forming_fluids.
Sindern, S., Kramm, U., 2000. Volume characteristics and element transfer of fenite aureoles: a case study from Iivaara alkaline complex, Finland. Lithos 51 (1), 75–93.
Sirqueira, A., Moura, M., Botelho, N., Kyser, T., 2018. Nature and evolution of paleoproterozoic Sn and rare metal albitites from Central Brazil: constraints based on textural, geochemical, Ar-Ar, and oxygen isotopes. Minerals 8 (9), 396.
Solodov, N.A., 1985. The Mineralo-Genesis of Rare Metal Formations. Niedra (in Ukrainian).
Suikkanen, E., Rämö, O.T., 2017. Metasomatic alkali-feldspar syenites (episyenites) of the Proterozoic Suomenniemi rapakivi granite complex, southeastern Finland. Lithos 294, 1–19.
Sviridov, V.V., 1973. Statistical investigations of chemistry within alkaline Oktiabrski Massif. Geologiia i Razvedka 5, 60–66.
Swamy, V., Muddle, B.C., Dai, Q., 2006. Size-dependent modifications of the Raman spectrum of rutile TiO_2. Applied Physics Letters 89. https://doi.org/10.1063/1.2364123 163,118.
Sylvester, P.J., 1989. Post-collisional alkaline granites. Journal of Geology 97 (3), 261–280.
Syme, R.W.G., Lockwood, D.J., Kerr, H.J., 1977. Raman spectrum of synthetic zircon ($ZrSiO_4$) and thorite ($ThSiO_4$). Journal of Physics C: Solid State Physics 10 (8), 1335–1348.
Tichonienkova, R.J., Osokin, J.D., Gonzjejev, A.A., 1967. Rare-metals Metasomatites of Alkaline Massives. Nauka (in Ukrainian).
Tomaschek, F., 2003. Zircons from syros, cyclades, greece-recrystallization and mobilization of zircon during high-pressure metamorphism. Journal of Petrology 44, 1977–2002.
Tuinstra, F., Koenig, J.L., 1970. Raman spectrum of graphite. The Journal of Chemical Physics 53, 1126–1130.
Van der Kerkhof, A.M., Thiéry, R., 2001. Carbonic inclusions. Lithos 55, 49–68.
Volkova, T.P., 2000. The genesis and ore mineralization of alkaline rocks from the Oktyabrskii Massif. Sb. Nauchn. Tr. 4, 9–10 (in Ukrainian).
Volkova, T.P., 2001. The Productivity Criterion of REE and Ore Mineralization within Rocks of the Oktyabrskii Massif Naukovi praci DonDTU. vol. 36 pp. 63–69 (in Ukrainian).
Wang, Y., Alsmeyer, D.C., Mccreery, R.L., 1990. Raman spectroscopy of carbon materials: Structural basis of observed spectra. Chemistry of Materials 2, 557–563.
Whalen, J.B., Currie, K.L., Chappell, B.W., 1987. A-types granites: geochemical characteristics, discrimination and petrogenesis. Contributions to Mineralogy and Petrology 95, 407–419.
White, W.B., Matsumara, M., Linnehan, D.G., Furukawa, T., Chandrasekhar, B.K., 1986. Absorption and luminescence of Fe^{3+} in single crystal orthoclase. American Mineralogist 71, 1415–1419.
Wopenka, B., Pasteris, J.D., 1993. Structural characterization of kerogens to granulite-facies 954 graphite: applicability of Raman microprobe spectroscopy. American Mineralogist 78, 533–557 5–955 6.
Xie, l., Wang, R., Chen, X., Qiu, J., Wang, D., 2005. Th-rich zircon from peralkaline a-type granite: mineralogicalfeatures and petrological implications. Chinese Science Bulletin 50, 809–817.
Yanchenko, V., Os'machko, L.S., Skobin, V.T., 2010. Mariupolits are synsheared phenomenon. Alkaline Rocks: Petrology, Mineralogy, Geochemistry. Proceedings of Conference, 19–21.09.2010. Semeneneko Institute of Geochemistry, Mineralogy and Ore Formations, Kiev, pp. 75–76.
Yang, W.B., Niu, H.C., Shan, Q., Sun, W.D., Zhang, H., Li, N.B., Jiang, Y.H., Yu, X.Y., 2014. Geochemistry of magmatic and hydrothermal zircon from the highly evolved Baerzhe alkaline granite: implications for Zr–REE–Nb mineralization. Mineralium Deposita 49 (4), 451–470.
Zhao, Z., Bao, Z., Qiao, Y., 2010. A peculiar composite M-and W-type REE tetrad effect: evidence from the Shuiquangou alkaline syenite complex, Hebei Province, China. Chinese Science Bulletin 55 (24), 2684–2696.
Zhenhua, Z., Xiaolin, X., Xiaodong, H., Yixian, W., Qiang, W., Zhiwei, B., Jahn, B., 2002. Controls on the REE tetrad effect in Evidence from the Qianlishan and Baerzhe granites: Granites, China. Geochemical Journal 36 (6), 527–543.